Inorganic Chemistry

Article

pubs.acs.org/IC

Pt(II) Bipyridyl Complexes Bearing Substituted Fluorenyl Motif on the Bipyridyl and Acetylide Ligands: Synthesis, Photophysics, and Reverse Saturable Absorption

Rui Liu,[†,∥] Yuhao Li,[†] Jin Chang,[‡] Eric R. Waclawik,[‡] and Wenfang Sun*[,†]

[†]Department of Chemistry and Biochemistry, North Dakota State University, Fargo, North Dakota 58108-6050, United States

[‡]Science and Engineering Faculty, Queensland University of Technology, 2 George Street, Brisbane, Queensland 4000, Australia

Supporting Information

ABSTRACT: A series of Pt(II) diimine complexes bearing benzothiazolylfluorenyl (BTZ-F_8), diphenylaminofluorenyl (NPh_2-F_8), or naphthalimidylfluorenyl (NI-F_8) motifs on the bipyridyl or acetylide ligands (**Pt-4**–**Pt-8**), (i.e., {4,4′-bis[7-R_1-F_8-(≡)$_n$-]bpy}Pt(7-R_2-F_8- ≡ -)$_2$, where F_8 = 9,9′-di(2-ethylhexyl)fluorene, bpy = 2,2′-bipyridine, **Pt-4**: R_1 = R_2 = BTZ, n = 0; **Pt-5**: R_1 = BTZ, R_2 = NI, n = 0; **Pt-6**: R_1 = R_2 = BTZ, n = 1; **Pt-7**: R_1 = BTZ, R_2 = NPh_2, n = 1; **Pt-8**: R_1 = NPh_2, R_2 = BTZ, n = 1) were synthesized. Their ground-state and excited-state properties and reverse saturable absorption performances were systematically investigated. The influence of these motifs on the photophysics of the complexes was investigated by spectroscopic methods and simulated by time-dependent density functional theory (TDDFT). The intense absorption bands below 410 nm for these complexes is assigned to predominantly $^1\pi,\pi^*$ transitions localized on either the bipyridine or the acetylide ligands; while the broad low-energy absorption bands between 420 and 575 nm are attributed to essentially ^{1}MLCT (metal-to-ligand charge transfer)/^{1}LLCT (ligand-to-ligand charge transfer) transitions, likely mixed with some ^{1}ILCT (intraligand charge transfer) transition for **Pt-4**–**Pt-7**, and predominantly ^{1}ILCT transition admixing with minor ^{1}MLCT/^{1}LLCT characters for **Pt-8**. The different substituents on the acetylide and bipyridyl ligands, and the degrees of π-conjugation in the bipyridyl ligand influence both the $^1\pi,\pi^*$ and charge transfer transitions pronouncedly. All complexes are emissive at room temperature. Upon excitation at their respective absorption band maxima, **Pt-4**, **Pt-6**, and **Pt-8** exhibit acetylide ligand localized $^1\pi,\pi^*$ fluorescence and ^{3}MLCT/^{3}LLCT phosphorescence in CH_2Cl_2, while **Pt-5** manifests ^{1}ILCT fluorescence and ^{3}ILCT phosphorescence. However, only ^{1}LLCT fluorescence was observed for **Pt-7** at room temperature. The nanosecond transient absorption study was carried out for **Pt-4**–**Pt-8** in CH_3CN. Except for **Pt-7** that contains NPh_2 at the acetylide ligands, **Pt-4**–**Pt-6** and **Pt-8** all exhibit weak to moderate excited-state absorption in the visible spectral region. Reverse saturable absorption (RSA) of these complexes was demonstrated at 532 nm using 4.1 ns laser pulses in a 2 mm cuvette. The strength of RSA follows this trend: **Pt-4** > **Pt-5** > **Pt-7** > **Pt-6** > **Pt-8**. Incorporation of electron-donating substituent NPh_2 on the bipyridyl ligand significantly decreases the RSA, while shorter π-conjugation in the bipyridyl ligand increases the RSA. Therefore, the substituent at either the acetylide ligands or the bipyridyl ligand could affect the singlet and triplet excited-state characteristics significantly, which strongly influences the RSA efficiency.

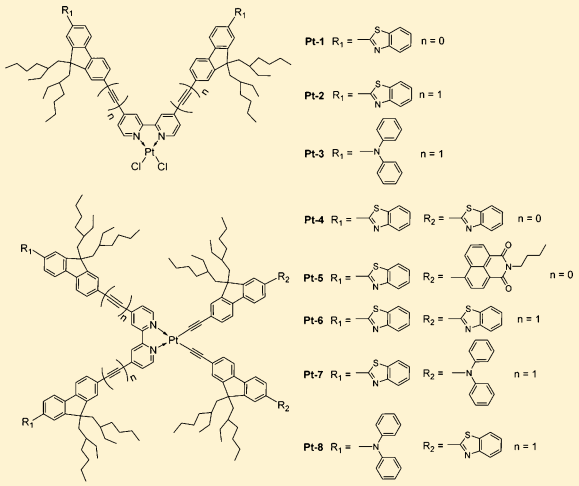

INTRODUCTION

Pt(II) diimine complexes[1] have attracted a great deal of interest in the past decade due to their unique photophysical properties and versatile potential applications, such as in low-power upconversion,[2−6] photoinduced charge separation,[7−9] luminescent materials,[10−12] chemosensors,[13,14] and nonlinear optics,[15,16] *etc*. Their rich photophysical properties and applications are intrinsically based on the presence of multiple charge transfer excited states, such as metal-to-ligand charge transfer (MLCT), ligand-to-ligand charge transfer (LLCT), intraligand charge transfer (ILCT), in addition to the ligand-localized π,π^* transitions. These features lead to long-lived triplet excited states, broadband excited-state absorption (ESA) in the visible to the near-IR region, and room temperature phosphorescence. More importantly, their photophysical properties can be readily tuned by modifying the ligand structures, which offers researchers the opportunity to design new Pt(II) diimine complexes with predetermined properties to tailor particular applications. It has been reported that variation

Received: March 20, 2014
Published: September 5, 2014

dx.doi.org/10.1021/ic500646r | *Inorg. Chem.* 2014, 53, 9516−9530

Chart 1. Structures of Ligands L-1−L-3, Zinc Complexes Zn-1−Zn-3, and Platinum Complexes Pt-1−Pt-8

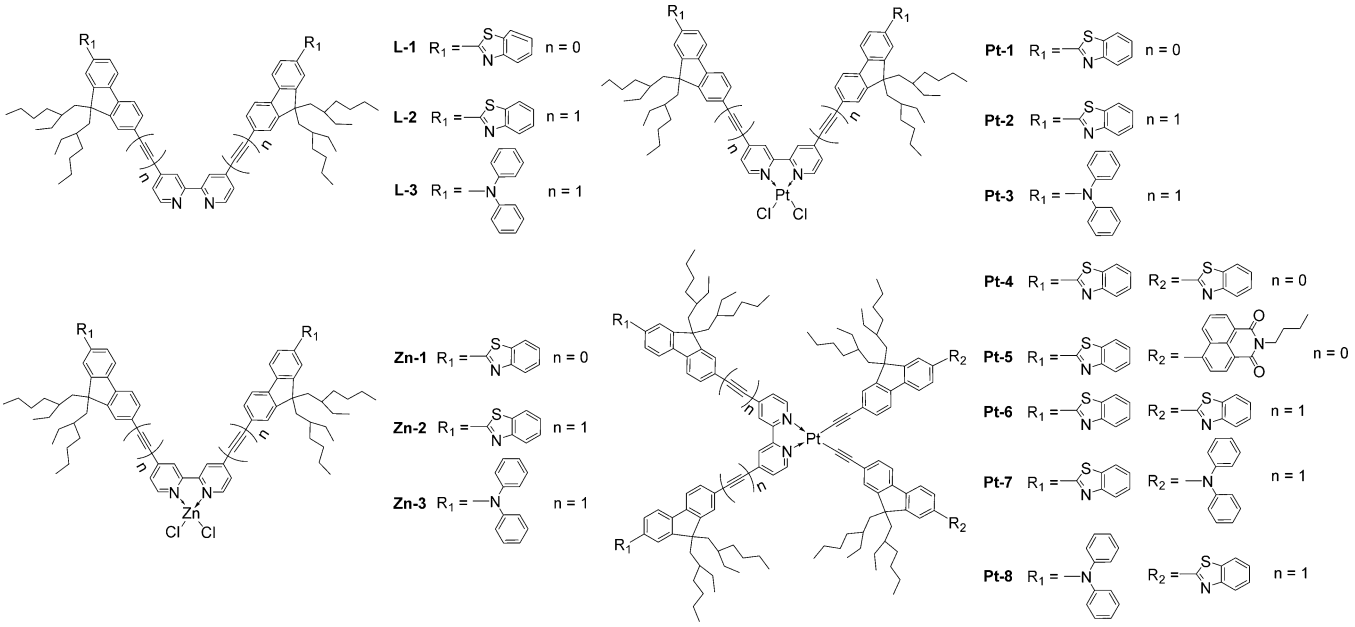

Scheme 1. Synthetic Routes for Ligands L-1−L-3, Zinc Complexes Zn-1−Zn-3, and Platinum Complexes Pt-1−Pt-8

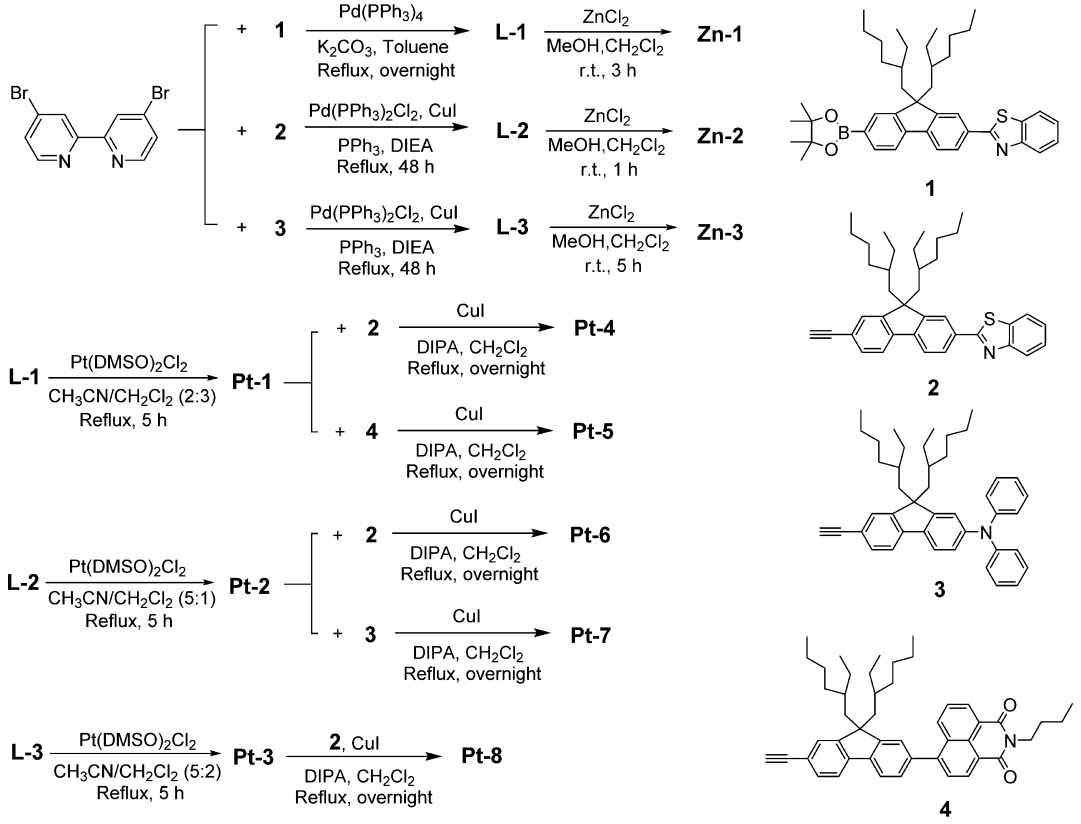

of the substituents on the bipyridine and/or the acetylide ligands could affect the photophysical properties of the Pt(II) diimine complexes drastically.[17−19] For example, the energy of the ^{1}MLCT band could be reduced significantly when the electron-withdrawing ability of the substituent on the bipyridine ligand increases. Meanwhile, the increased electron-donating ability of the substituent on the acetylide ligands could also decrease the energy of the ^{1}MLCT state. However, the influence of the substituents on the acetylide ligands does not follow a monotonic trend on the energy, lifetime, and quantum yield of the lowest triplet excited state because of the interplay of multiple excited states in proximity. It has been reported in the literature that by modification of the acetylide ligands the lowest triplet excited state of the Pt(II) diimine complexes could be tuned to a ^{3}MLCT state,[10] a $^3\pi,\pi$ state localized on two acetylide ligands,[19] a $^3\pi,\pi$ state localized on

dx.doi.org/10.1021/ic500646r | Inorg. Chem. 2014, 53, 9516−9530

one of the acetylide ligands,[20] or a mixture of the ^{3}MLCT and $^3\pi,\pi$ states.[12] Our group discovered that strong electron-donating substituents such as the diphenylamino group and strong electron-withdrawing substituents such as the nitro group on the acetylide ligands could change the nature of the lowest triplet excited state from a charge transfer triplet excited state to predominantly acetylide ligand-localized $^3\pi,\pi$ state.[21,22] Furthermore, the lowest triplet excited state could be switched from a $^3\pi,\pi$ state to a ^{3}MLCT state in solvent with different polarities.[11]

In addition to the aforementioned structure−property correlation studies, in recent years our group investigated the effects of extending the π-conjugation of the acetylide ligands on the Pt(II) bipyridyl complexes bearing benzothiazolyl (BTZ)- and naphthalimide (NI)-substituted fluorenylacetylide ligands[15,21,23] and on the complexes with diphenylamino- and nitro-substituted phenylethynylfluorenylacetylide ligands.[24] It was revealed that extending the π-conjugation of the acetylide ligands could increase the lifetime of the triplet excited state and enhance the reverse saturable absorption (RSA) at 532 nm for ns laser pulses. Zhao and co-workers also reported the long-lived triplet excited state in Pt(II) bipyridyl complexes with extended π-conjugated acetylide ligands.[6] Although these results are quite interesting, studies on the Pt(II) diimine complexes with extended π-conjugated substituents on both the diimine ligand and acetylide ligands have been quite scarce except for our very recent work on Pt(II) complexes with benzothiazolylfluorenyl substituents on both of the bipyridyl and acetylide ligands.[25] Our study discovered that the triplet excited-state lifetime of the Pt(II) diimine complexes was dramatically increased to ∼60 μs and the triplet excited-state absorption spectrum became much broader upon extending the π-conjugation on both the diimine and acetylide ligands; thus, the complexes exhibited very strong RSA at 532 nm. Intrigued by this preliminary study, we are interested in further understanding the effect of introducing aromatic electron-donating or -withdrawing substituents on the π-conjugated fluorenyl groups that are attached to the diimine and acetylide ligands. Understanding how the nature and position of these substituents influence the photophysics of Pt(II) complexes is essential for rational design of Pt(II) complexes as efficient photonic materials, such as reverse saturable absorbing materials.

To reach this goal, in this work, we designed and synthesized a series of novel Pt(II) diimine complexes bearing different arylfluorenyl components on both the acetylide and bipyridine ligands (**Pt-4**−**Pt-8** in Chart 1). The BTZ and NI groups were chosen as electron-withdrawing substituents, while the NPh_2 group was selected as an electron-donating substituent. To aid in our understanding of the photophysics of **Pt-4**−**Pt-8**, three zinc diimine chloride complexes (**Zn-1**−**Zn-3** in Chart 1) and three Pt(II) diimine chloride complexes (**Pt-1**−**Pt-3** in Chart 1) with the corresponding diimine ligand were synthesized as reference complexes. For all complexes, 2-ethylhexyl substituents were introduced on the fluorene units in order to reduce the intermolecular aggregation and improve the solubility of the Pt complexes. The synthetic routes for the ligands **L-1**−**L-3** and for all of the target complexes are illustrated in Scheme 1. The photophysics of the ligands and the complexes, and the RSA of the Pt(II) complexes, were systematically investigated with the aim of understanding the structure−property correlations for developing efficient reverse saturable absorbers.

EXPERIMENTAL SECTION

Synthesis and Characterization. All solvents and reagents for synthesis were purchased from Aldrich or Alfa Aesar and used as is unless otherwise stated. The precursors **1**−**4** were prepared according to the literature procedures.[21,23,26,27] Spectrophotmetric grade solvents were used for spectroscopic studies and were purchased from Alfa Aesar Company and used without further purification. Silica gels used for chromatography were purchased from Alfa Aesar Company (230−400 mesh). Tetrahydrofuran (THF), diethylamine (DEA), diisopropylamine (DIPA), and *N*,*N*-diisopropylethylamine (DIEA) were distilled under N_2 over sodium benzophenone ketyl. The ligands and complexes were characterized by ^{1}H NMR, HRMS, and elemental analyses. ^{1}H NMR spectra were obtained on a Varian Oxford-400 VNMR spectrometer or a Varian Oxford-500 VNMR spectrometer. HRMS data for ligands **L-1**−**L-3** and Pt complexes **Pt-1**−**Pt-3** were obtained on a Bruker BioTOF III mass spectrometer. The Zn complexes **Zn-1**−**Zn-3** and the Pt complexes **Pt-4**−**Pt-8** were unable to be ionized using the ESI technique. Therefore, their mass analyses were performed on an Applied Biosystems Voyager-DE STR MALDI-TOF mass spectrometer, which is equipped with a nitrogen laser (337 nm, 3 ns pulse, 20 Hz maximum firing rate) and was operated in the reflection mode. 2′,4′,6′-Trihydroxyacetophenone monohydrate (THAP) was used as the matrix. Elemental analyses were carried out by NuMega Resonance Laboratories, Inc. in San Diego, California.

L-1. 4,4′-Dibromo-2,2′-bipyridine (0.44 g, 1.40 mmol), compound **1** (0.2 g, 0.31 mmol) and $Pd(PPh_3)_4$ (0.16 g, 0.14 mmol) were added to 30 mL of toluene in a round-bottom flask. Then 7 mL of 2 M K_2CO_3 aqueous solution was added. The mixture was heated to reflux under argon for overnight. The volume of this mixture was then reduced in vacuo and the residue was extracted with CH_2Cl_2. The CH_2Cl_2 layer was washed with brine and dried over $MgSO_4$. After removal of the solvent, the crude product was purified by column chromatography (neutral Al_2O_3, hexane/EtOAc = 10:1, v/v), then recrystallized from acetone to afford white solid 0.50 g (yield: 30%). ^{1}H NMR (400 MHz, $CDCl_3$): δ 9.85 (d, J = 7.2 Hz, 2H), 8.26−8.12 (m, 8H), 7.92−7.90 (m, 6H), 7.84−7.79 (m, 6H), 7.54 (t, J = 6.2 Hz, 2H), 7.43 (t, J = 6.2 Hz, 2H), 2.24−2.10 (m, 8H), 0.92−0.75 (m, 32H), 0.64−0.54 (m, 28H). ESI-HRMS: m/z calc for $[C_{82}H_{94}N_4S_2 + H]^+$: 1199.6993; Found: 1199.7041. Anal. Calcd (%) for $C_{82}H_{94}N_4S_2$: C, 82.09; H, 7.90; N, 4.67. Found: C, 81.87; H, 8.38; N, 4.27.

L-2. A stirred suspension of 4,4′-dibromo-2,2′-bipyridine (0.27 g, 0.87 mmol), compound **2** (1.00 g, 1.82 mmol), PPh_3 (0.046 g, 0.18 mmol), $Pd(PPh_3)Cl_2$ (0.06 g, 0.09 mmol), and CuI (0.01 g, 0.045 mmol) in DIEA (20 mL) was deoxygenated with argon at r.t. and then heated to reflux for 48 h. The volume of the mixture was then reduced in vacuo, and the residue was extracted with ether. The combined ether layer was washed with brine and dried over $MgSO_4$. After removal of the solvent, the residue was purified by column chromatography (neutral Al_2O_3, hexane/CH_2Cl_2 = 2:1 then 1:1, v/v) to afford the crude product as a yellow oil. Then the yellow oil was recrystallized from acetone to afford yellow solid 0.27g (yield: 25%). ^{1}H NMR (400 MHz, $CDCl_3$): δ 8.68 (d, J = 7.2 Hz, 2H), 8.57 (s, 2H), 8.13−8.06 (m, 6H), 7.89 (d, J = 7.6 Hz, 2H), 7.80−7.74 (m, 4H), 7.60−7.56 (m, 4H), 7.50−7.44 (m, 4H), 7.38−7.35 (m, 2H), 2.10−2.06 (m, 8H), 0.92−0.69 (m, 36H), 0.59−0.48 (m, 24H). ESI-HRMS: m/z calc for $[C_{86}H_{94}N_4S_2 + H]^+$: 1247.6993; Found: 1247.6992. Anal. Calcd (%) for $C_{86}H_{94}N_4S_2$: C, 82.78; H, 7.59; N, 4.49. Found: C, 83.05; H, 8.08; N, 4.55.

L-3. A stirred suspension of 4,4′-dibromo-2,2′-bipyridine (0.31 g, 0.98 mmol), compound **3** (1.20 g, 2.06 mmol), PPh_3 (0.051g, 0.196 mmol), $Pd(PPh_3)Cl_2$ (0.068 g, 0.098 mmol), and CuI (0.01 g, 0.049 mmol) in DIEA (20 mL) was deoxygenated with argon at r.t. and then heated to reflux for 48 h. The volume of the mixture was then reduced *in vacuo*, and extracted with ether. The combined ether layer was washed with brine and dried over $MgSO_4$. After removal of the solvent, the crude product was purified by column chromatography (neutral Al_2O_3, hexane/CH_2Cl_2 = 10:1, v/v) to afford 0.27 g red solid as the product (yield: 21%). ^{1}H NMR (400 MHz, $CDCl_3$): δ 8.68 (d, J = 7.2 Hz, 2H), 8.57 (s, 2H), 7.61−7.48 (m, 8H), 7.38−7.42 (m, 2H),

dx.doi.org/10.1021/ic500646r | Inorg. Chem. 2014, 53, 9516−9530

7.29−7.20 (m, 4H), 7.08−7.04 (m, 20H), 2.10−2.06 (m, 8H), 0.92−0.69 (m, 40H), 0.59−0.48 (m, 20H). ESI-HRMS: *m*/*z* calc for $[C_{96}H_{106}N_4 + H]^+$: 1315.8490; Found: 1315.8519. Anal. Calcd (%) for $C_{96}H_{106}N_4$: C, 87.62; H, 8.12; N, 4.26. Found: C, 87.23; H, 8.12; N, 4.27.

Zn-1. Compounds $ZnCl_2$ (7.95 mg, 0.058 mmol) and **L-1** (70 mg, 0.058 mmol) were dissolved in 10 mL of mixed dichloromethane and methanol (v/v = 1:1), and the solution was stirred at room temperature for 3 h. Then the solvent was removed, and the crude product was recrystallized from hexane/acetone to give 40 mg yellowish-green solid (yield: 51%). ^{1}H NMR (400 MHz, $CDCl_3$): δ 8.90 (d, J = 4.8 Hz, 2H), 8.48 (s, 2H), 8.19−8.08 (m, 6H), 7.96−7.88 (m, 8H), 7.78−7.62 (m, 4H), 7.50 (t, J = 7.6 Hz, 2H), 7.39 (t, J = 7.6 Hz, 2H), 2.22−2.09 (m, 8H), 0.90−0.69 (m, 32H), 0.58−0.50 (m, 28H). MALDI-TOF HRMS: *m*/*z* calc for $[C_{82}H_{94}N_4S_2ClZn + 2H]^+$: 1299.6056; Found: 1299.5953. Anal. Calcd (%) for $C_{82}H_{94}Cl_2N_4S_2Zn\cdot CH_2Cl_2\cdot 0.5C_6H_{14}$: C, 70.54; H, 7.11; N, 3.83. Found: C, 70.17; H, 7.51; N, 3.97.

Zn-2. Compounds $ZnCl_2$ (7.6 mg, 0.056 mmol) and **L-2** (70 mg, 0.056 mmol) were dissolved in 10 mL of mixed dichloromethane/methanol (v/v = 1:1), and the solution was stirred at room temperature for 1 h. Then the solvent was removed, and the crude product was recrystallized from acetone to yield 40 mg yellowish-green solid as the product (yield: 52%). ^{1}H NMR (400 MHz, $CDCl_3$): δ 8.86 (d, J = 5.0 Hz, 2H), 8.38 (m, 2H), 8.20−8.12 (m, 6H), 7.96 (d, J = 8.0 Hz, 2H), 7.89−7.83 (m, 6H), 7.72−7.68 (m, 4H), 7.54 (t, J = 7.5 Hz, 2H), 7.43 (t, J = 7.5 Hz, 2H), 2.22−2.09 (m, 8H), 0.97−0.73 (m, 40H), 0.64−0.55 (m, 20H). MALDI-TOF HRMS: *m*/*z* calc for $[C_{86}H_{94}N_4S_2ClZn + 2H]^+$: 1347.6056; Found: 1347.5834. Anal. Calcd (%) for $C_{86}H_{94}N_4S_2Cl_2Zn\cdot H_2O$: C, 73.66; H, 6.92; N, 4.00. Found: C, 73.80; H, 7.00; N, 4.05.

Zn-3. Compounds $ZnCl_2$ (8.3 mg, 0.061 mmol) and **L-3** (80 mg, 0.061 mmol) were dissolved in 10 mL of mixed dichloromethane/methanol (v/v = 1:1), and the solution was stirred at room temperature for 5 h. Then the solvent was removed, and the crude product was recrystallized from hexane/EtOH to afford 65 mg red solid as the product (yield: 74%). ^{1}H NMR (500 MHz, $CDCl_3$): δ 8.75 (s, 2H), 8.50 (s, 2H), 7.66−7.55 (m, 10H), 7.26 (m, 2H), 7.13−7.04 (m, 22H), 1.97−1.86 (m, 8H), 1.05−0.74 (m, 40H), 0.60−0.54 (m, 20H). MALDI-TOF HRMS: *m*/*z* calc for $[C_{96}H_{106}N_4ClZn]^+$: 1415.7509; Found: 1415.7457. Anal. Calcd (%) for $C_{96}H_{106}N_4Cl_2Zn\cdot C_3H_6O\cdot 2H_2O$: C, 76.89; H, 7.58; N, 3.62. Found: C, 77.05; H, 7.96; N, 3.74.

Pt-1. Compounds $Pt(DMSO)_2Cl_2$ (70.4 mg, 0.167 mmol) and **L-1** (200 mg, 0.167 mmol) were added to a mixed solution of 20 mL CH_3CN and 30 mL CH_2Cl_2, and the solution was heated to reflux for 5 h. After removal of the solvent, the crude product was purified by column chromatography (silica gel, hexane/CH_2Cl_2 = 1:1, v/v, then CH_2Cl_2) and then by recrystallization from CH_2Cl_2/Et_2O to afford 50 mg yellow solid as the product (yield: 20%). ^{1}H NMR (400 MHz, $CDCl_3$): δ 9.76 (d, J = 6.0 Hz, 2H), 8.24−8.07 (m, 8H), 7.95−7.87 (m, 6H), 7.82−7.78 (m, 4H), 7.72 (d, J = 4.8 Hz, 2H), 7.48 (t, J = 7.6 Hz, 2H), 7.38 (t, J = 7.6 Hz, 2H), 2.23−2.09 (m, 8H), 0.98−0.70 (m, 32H), 0.62−0.50 (m, 28H). ESI-HRMS: *m*/*z* calc for $[C_{82}H_{94}N_4S_2PtCl_2 + Na]^+$: 1487.5841; Found: 1487.5868. Anal. Calcd (%) for $C_{82}H_{94}Cl_2N_4S_2Pt$: C, 67.19; H, 6.46; N, 3.82. Found: C, 66.84; H, 6.90; N, 3.60.

Pt-2. Compounds $Pt(DMSO)_2Cl_2$ (67.6 mg, 0.160 mmol) and **L-2** (200 mg, 0.160 mmol) were added to 50 mL of CH_3CN and 10 mL of CH_2Cl_2, and the solution was heated to reflux for 5 h. After removal of the solvent, the crude product was recrystallized from CH_2Cl_2/hexane to afford 170 mg yellow solid as the product (yield: 70%). ^{1}H NMR (400 MHz, $CDCl_3$): δ 9.82 (d, J = 6.0 Hz, 2H), 8.13−8.05 (m, 8H), 7.90 (d, J = 8.4 Hz, 2H), 7.84−7.79 (m, 4H), 7.66−7.62 (m, 6H), 7.49 (t, J = 7.8 Hz, 2H), 7.38 (t, J = 7.8 Hz, 2H), 2.22−2.09 (m, 8H), 0.97−0.69 (m, 40H), 0.59−0.50 (m, 20H). ESI-HRMS: *m*/*z* calc for $[C_{86}H_{94}N_4S_2PtCl_2 + Na]^+$: 1535.5842; Found: 1535.5802. Anal. Calcd (%) for $C_{86}H_{94}Cl_2N_4PtS_2\cdot{}^1/_3CH_2Cl_2$: C, 67.24; H, 6.20; N, 3.63. Found: C, 67.40; H, 6.47; N, 3.66.

Pt-3. Compounds $Pt(DMSO)_2Cl_2$ (64.2 mg, 0.152 mmol) and **L-3** (230 mg, 0.152 mmol) were added to 50 mL of CH_3CN and 20 mL of CH_2Cl_2, and the solution was heated to reflux for 5 h. After removal of the solvent, the crude product was purified by column chromatography (neutral Al_2O_3, hexane/EtOAc = 4:1 then 2:1, v/v) to afford 101 mg reddish-brown solid (yield: 42%). ^{1}H NMR (400 MHz, $CDCl_3$): δ 9.77 (d, J = 6.4 Hz, 2H), 8.20−7.95 (m, 3H), 7.80−7.42 (m, 11H), 7.25−7.21 (m, 10H), 7.09−7.01 (m, 12H), 2.22−1.79 (m, 8H), 1.05−0.70 (m, 40H), 0.55−0.51 (m, 20H). ESI-HRMS: *m*/*z* calc for $[C_{96}H_{106}Cl_2N_4Pt + Na]^+$: 1603.7344; Found: 1603.7380. Anal. Calcd (%) for $C_{96}H_{106}Cl_2N_4Pt$: C, 72.89; H, 7.06; N, 3.53. Found: C, 73.19; H, 7.16; N, 3.59.

Pt-4. To a degassed solution of **Pt-1** (100 mg, 0.068 mmol) and **2** (78 mg, 0.143 mmol) in dry CH_2Cl_2 (30 mL) and diisopropylamine (20 mL) was added CuI (1.6 mg, 0.0084 mmol). The mixture was refluxed under argon for overnight. After removal of the solvent, the crude product was purified by column chromatography (silica gel, hexane/CH_2Cl_2 = 2:1, then 1:1, v/v), and recrystallized from CH_2Cl_2/EtOH to afford 89 mg red solid (yield: 53%). ^{1}H NMR (400 MHz, $CDCl_3$): δ 9.99 (s, 2H), 8.32 (s, 2H), 8.16−7.95 (m, 12H), 7.93−7.83 (m, 8H), 7.80−7.72 (m, 8H), 7.64−7.58 (m, 6H), 7.49−7.44 (m, 4H), 7.40−7.32 (m, 4H), 2.22−2.01 (m, 16H), 0.98−0.50 (m, 120H). MALDI-TOF HRMS: *m*/*z* calc for $[C_{158}H_{182}N_6S_4Pt]^+$: 2487.2990; Found: 2487.2571. Anal. Calcd (%) for $C_{158}H_{182}N_6S_4Pt\cdot{}^1/_2CH_2Cl_2\cdot H_2O$: C, 74.68; H, 7.32; N, 3.30. Found: C, 74.69; H, 7.67; N, 3.12.

Pt-5. To a degassed solution of **Pt-1** (60 mg, 0.041 mmol) and **4** (58.5 mg, 0.086 mmol) in dry CH_2Cl_2 (30 mL) and diisopropylamine (20 mL) was added CuI (1.0 mg, 0.0053 mmol). The mixture was refluxed under argon for overnight. After removal of the solvent, the crude product was purified by column chromatography (silica gel, CH_2Cl_2, then CH_2Cl_2/EtOAc = 4:1, v/v) to afford 49.6 mg red solid (yield: 40%). ^{1}H NMR (400 MHz, $CDCl_3$): δ 9.89 (s, 2H), 8.63 (t, J = 7.2 Hz, 4H), 8.35−8.26 (m, 4H), 8.19−8.13 (m, 4H), 8.09 (d, J = 8.0 Hz, 2H), 7.91−7.64 (m, 24H), 7.52−7.37 (m, 8H), 4.17 (t, J = 7.6 Hz, 4H), 2.23−2.03 (m, 16H), 1.75−1.71 (m, 4H),1.47−1.42 (m, 4H), 0.99−0.75 (m, 80H), 0.65−0.51 (m, 46H). MALDI-TOF HRMS: *m*/*z* calc for $[C_{176}H_{202}N_6O_4PtS_2 + H]^+$: 2724.4989; Found: 2724.4324. Anal. Calcd (%) for $C_{176}H_{202}N_6O_4PtS_2\cdot CH_2Cl_2\cdot 2H_2O$: C, 74.70; H, 7.31; N, 2.95. Found: C, 74.60; H, 7.80; N, 2.87.

Pt-6. To a degassed solution of **Pt-2** (200 mg, 0.132 mmol) and **2** (152 mg, 0.277 mmol) in dry CH_2Cl_2 (30 mL) and diisopropylamine (20 mL) was added CuI (1.3 mg, 0.007 mmol). The mixture was refluxed under argon for overnight. After removal of the solvent, the crude product was purified by column chromatography (silica gel, hexane/CH_2Cl_2 = 1:1, then 1:2, v/v) to afford 120 mg purple solid (yield: 36%). ^{1}H NMR (400 MHz, $CDCl_3$): δ 9.90 (d, J = 6.4 Hz, 4H), 8.21−8.04 (m, 14H), 7.91−7.79 (m, 8H), 7.72 (d, J = 8.0 Hz, 2H), 7.65−7.51 (m, 10H), 7.48−7.44 (m, 4H), 7.40−7.33 (m, 4H), 2.17−2.04 (m, 16H), 1.03−0.71 (m, 80H), 0.58−0.50 (m, 40H). MALDI-TOF HRMS: *m*/*z* calc for $[C_{162}H_{182}N_6S_4Pt]^+$: 2535.2990; Found: 2535.2400. Anal. Calcd (%) for $C_{162}H_{182}N_6S_4Pt\cdot CH_2Cl_2\cdot Et_2O$: C, 74.41; H, 7.25; N, 3.12. Found: C, 74.28; H, 7.66; N, 2.94.

Pt-7. To a degassed solution of **Pt-2** (70 mg, 0.046 mmol) and **3** (56 mg, 0.097 mmol) in dry CH_2Cl_2 (30 mL) and diisopropylamine (20 mL) was added CuI (0.43 mg, 0.0023 mmol). The mixture was refluxed under argon for overnight. After reaction, the mixture was washed with brine and dried over $MgSO_4$. After removal of the solvent, the crude product was purified by column chromatography (silica gel, hexane/CH_2Cl_2 = 1:1, then 1:2, v/v) to afford dark-black solid. Further recrystallization from CH_2Cl_2/CH_3CN yielded 32 mg black solid (yield: 27%). ^{1}H NMR (400 MHz, $CDCl_3$): δ 9.93 (d, J = 5.6 Hz, 2H), 8.16−8.09 (m, 8H), 8.08 (d, J = 8.4 Hz, 2H), 7.82−7.79 (m, 4H), 7.69−7.62 (m, 6H), 7.53−7.47 (m, 10H), 7.38 (d, J = 7.6 Hz, 2H), 7.23−7.18 (m, 8H), 7.07−7.04 (m, 10H), 7.02−6.95 (m, 6H), 2.04−1.98 (m, 16H), 1.02−0.70 (m, 80H), 0.60−0.50 (m, 40H). MALDI-TOF HRMS: *m*/*z* calc for $[C_{172}H_{194}N_6PtS_2 + H]^+$: 2604.4566; Found: 2604.1260. Anal. Calcd (%) for $C_{172}H_{194}N_6PtS_2$: C, 79.31; H, 7.51; N, 3.23. Found: C, 79.29; H, 7.80; N, 3.20.

Pt-8. To a degassed solution of **Pt-3** (50 mg, 0.032 mmol) and **2** (36 mg, 0.066 mmol) in dry CH_2Cl_2 (30 mL) and diisopropylamine

dx.doi.org/10.1021/ic500646r | *Inorg. Chem.* 2014, 53, 9516−9530

(20 mL) was added CuI (0.5 mg, 0.0026 mmol). The mixture was refluxed under argon for overnight. After reaction, the mixture was washed with brine and dried over $MgSO_4$. Then the solvent was removed, and the crude product was purified by column chromatography (silica gel, hexane/CH_2Cl_2 = 1:1, then 1:2, v/v) to afford dark-black solid. Further recrystallization from acetone/CH_3CN yielded 15 mg black solid (yield: 18%). ^{1}H NMR (400 MHz, $CDCl_3$): δ 9.93 (d, J = 5.6 Hz, 2H), 8.15–8.04 (m, 10H), 7.88 (d, J = 8.0 Hz, 2H), 7.72 (d, J = 8.0 Hz, 2H), 7.65–7.55 (m, 16H), 7.46 (t, J = 8.0 Hz, 2H), 7.34 (t, J = 8.0 Hz, 2H), 7.25–7.21 (m, 8H), 7.08–7.01 (m, 14H), 2.14–1.79 (m, 16H), 1.01–0.63 (m, 80H), 0.63–0.49 (m, 40H). MALDI-TOF HRMS: m/z calc for $[C_{172}H_{194}N_6PtS_2 + H]^+$: 2604.4566; Found: 2604.4666. Anal. Calcd (%) for $C_{172}H_{194}N_6PtS_2 \cdot {}^1/_2CH_2Cl_2$: C, 78.27; H, 7.43; N, 3.17. Found: C, 78.01; H, 7.85; N, 3.12.

Photophysical Measurements. The UV–vis absorption spectra were recorded on a Shimadzu UV-2501 spectrophotometer. The emission spectra were measured on a FluoroMax-4 fluorometer/phosphorometer. The emission quantum yields were obtained by the relative actinometry method[28] in solutions. A degassed aqueous solution of $[Ru(bpy)_3]Cl_2$ (Φ_{em} = 0.042, λ_{ex} = 436 nm)[29] was used as the reference for the Pt complexes **Pt-4**–**Pt-8**, and an aqueous solution of quinine sulfate (Φ_{em} = 0.546, λ_{ex} = 365 nm)[30] was used as the reference for the ligands, zinc complexes, and the Pt(II) chloride complexes **Pt-1**–**Pt-3**. The nanosecond transient absorption (TA) spectra, triplet excited-state lifetimes, and triplet excited-state quantum yields were measured on an Edinburgh LP920 laser flash photolysis spectrometer. The excitation source was the third harmonic output (355 nm) of a Nd:YAG laser (Quantel Brilliant, pulsewidth ~4.1 ns; the repetition rate was set up to 1 Hz). Before each measurement, the sample solutions were degassed with Ar for 30 min.

Singlet depletion method[31] was used to determine the triplet excited-state molar extinction coefficients (ε_T) at the TA band maximum. The triplet excited-state quantum yield was calculated by the relative actinometry[32] using the ε_T value obtained from the singlet depletion method and silicon 2,3-naphthalocyanine bis-(trihexylsilyloxide) (SiNc) in benzene as the reference (ε_{590} = 70,000 $M^{-1}\cdot cm^{-1}$, Φ_T = 0.20).[33]

DFT Calculations. The ground electronic state frontier molecular orbitals (FMOs) of complexes **Pt-4**–**Pt-8** were simulated by density functional theory (DFT), and their excited electronic states were calculated using the time-dependent density functional theory (TDDFT) method. The specific DFT method used was PBE1PBE[34–36] for calculating excited electronic states. The basis sets used in all calculations were the 6-31G* set[37–41] for all light atoms and the LANL2DZ set[42–44] for the Pt atom. Full equilibrium geometry optimizations were performed for the ground electronic states of all complexes. However, a methyl group was used to replace the 2-ethylhexyl group in Pt complexes to simplify the calculations due to the size of the complexes. Excited-state calculations for 20 excited states were performed at the fully optimized ground-state molecular geometry of the complexes. All the calculations were performed with Gaussian 09 software package.[45]

Nonlinear Transmission Measurement. The experimental setup and details have been reported previously.[46] A plano-convex lens (f = 40 cm) was used to focus the beam to the sample cuvette. The radius of the beam waist at the focal point was approximately 96 μm. A Quantel Brilliant nanosecond laser (4.1 ns pulses) with a repetition rate of 10 Hz was used as the light source.

RESULTS AND DISCUSSION

Synthesis. Scheme 1 outlines the synthetic routes for ligands **L-1**–**L-3**, and complexes **Zn-1**–**Zn-3**, and **Pt-1**–**Pt-8**. The synthesis of the key precusors **1**–**4** follows the reported procedures.[21,23,26,27] The Suzuki or Sonogashira cross-coupling reaction was employed to synthesize ligands **L-1**–**L-3**. **Zn-1**–**Zn-3** were synthesized by the reaction of ligands **L-1**–**L-3** with $ZnCl_2$ at room temperature. Refluxing **L-1**–**L-3** with Pt-$(DMSO)_2Cl_2$ in CH_3CN/CH_2Cl_2 mixture yielded **Pt-1**–**Pt-3**. Then substitution of the Cl coligands in **Pt-1**–**Pt-3** by the respective arylfluorenylacetylide ligands **2**–**4** in the presence of CuI and diisopropylamine (DIPA) gave Pt complexes **Pt-4**–**Pt-8**. All Zn and Pt complexes are air-stable and soluble in common organic solvents, such as CH_2Cl_2, $CHCl_3$, acetone, tetrahydrofuran, toluene, DMF, and DMSO. The structures and purity of the ligands and complexes were characterized by ^{1}H NMR spectroscopy, high-resolution mass spectrometry, and elemental analyses. Upon coordination with the Zn(II) and Pt(II) metal ions and exchange of chloride with acetylide as the coligands, informative bipyridine resonances (δ 7.8–9.9 ppm) were observed because they shifted substantially to downfield, especially the protons adjacent to the coordination sites.

Electronic Absorption. The UV–vis absorption spectra of **L-1**–**L-3**, **Zn-1**–**Zn-3**, and **Pt-1**–**Pt-8** were measured in CH_2Cl_2 solutions at different concentrations. No ground-state aggregation was observed in the concentration range investigated (1×10^{-6} to 1×10^{-4} mol/L), which is reflected by the compliance of the absorbance with the Beer's law. The absorption spectra of the ligands and the complexes in CH_2Cl_2 are presented in Figure 1, and their absorption band maxima

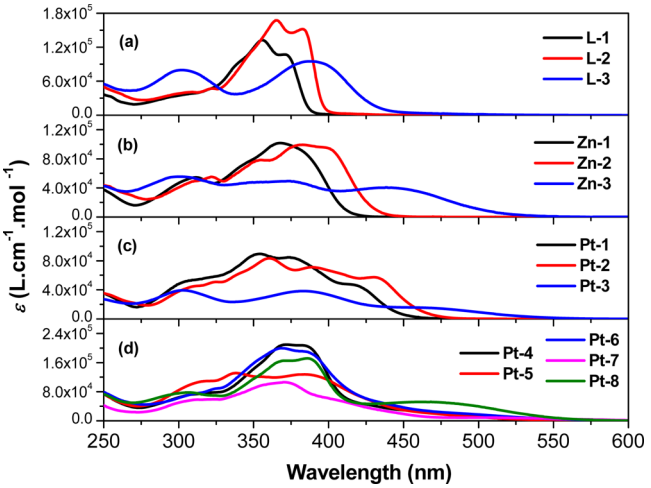

Figure 1. UV–vis absorption spectra of (a) ligands **L-1**–**L-3**; (b) Zn complexes **Zn-1**–**Zn-3**; (c) Pt chloride complexes **Pt-1**–**Pt-3**; and (d) Pt acetylide complexes **Pt-4**–**Pt-8**. All of the spectra were measured in CH_2Cl_2.

and molar extinction coefficients are listed in Table 1. For ligands **L-1** and **L-2**, each of them exhibits structured major absorption bands between 350 and 400 nm, which should be attributed to the $^1\pi,\pi^*$ transitions within the molecule. Because of the extended conjugation via the triple bonds in **L-2**, its band maxima are red-shifted, and molar extinction coefficients are larger in comparison to those of **L-1**. In contrast, ligand **L-3** that contains the strong electron-donating substituent NPh_2 shows two broad, featureless absorption bands at 302 and 387 nm, respectively, which could be assigned to the $^1\pi,\pi^*$ transitions. However, the 387 nm band possibly admixes some intraligand charge transfer (^{1}ILCT, $\pi(NPh_2$-fluorene) → π^*(bpy)) characters. After complexation with Zn(II), the major absorption bands of **Zn-1** and **Zn-2** (Figure 1b) become broader, less structured, and somewhat red-shifted in comparison to their respective ligands (Figure 1a), accompanied by the appearance of a tail above 400 nm. These features could be attributed to the increased ^{1}ILCT character in the Zn complexes. Complexation of the bipyridine (bpy) ligand with

dx.doi.org/10.1021/ic500646r | Inorg. Chem. 2014, 53, 9516–9530

Table 1. Photophysical Parameters of L-1−L-3, Zn-1−Zn-3, and Pt-1−Pt-8

	λ_{abs}/nm (ε/10^3·L·mol^{-1}·cm^{-1})[a]	λ_{em}/nm (τ_{em}/ns; Φ_{em}) r.t.[b]	λ_{em}/nm (τ_{em}/μs) 77 K[d]	$\lambda_{T1\text{-}Tn}$/nm (τ_{TA}/μs; $\varepsilon_{T1\text{-}Tn}$/$10^4$·L·mol^{-1}·cm^{-1}; Φ_T)[f]
L-1	356 (13.2), 370 (10.7)	388, 408 (*c*; 0.71), 429	387, 409, 434 (*e*)	555 (9.4, −, −)
L-2	322 (46.7), 365 (167.4), 382 (152.2)	394, 414 (*c*; 0.79), 435	398, 418, 443 (*e*)	585 (63.0, −, −)
L-3	302 (79.8), 387 (95.0)	496 (*c*; 0.51)	461 (*e*)	*e*
Zn-1	311 (54.5), 368 (101.6)	459 (*c*; 0.78)	386, 408, 428 (*e*)	565 (19.5, 16.0, 0.018)
Zn-2	322 (55.1), 354 (78.2), 382 (99.2)	491 (*c*; 0.61)	397, 418, 441 (*e*)	530 (36.0, 5.76, 0.033)
Zn-3	300 (55.6), 374 (49.4), 438 (40.7)	500 (*c*; 0.02)	513 (*e*)	*e*
Pt-1	354 (89.6), 417 (46.9)	463 (*c*; 0.07)	556, 600 (*e*)	530 (6.6, 4.82, 0.13)
Pt-2	360 (83.3), 389 (71.0), 430 (57.3)	491 (*c*; 0.006)	571, 615 (*e*)	545 (11.1, 5.64, 0.09)
Pt-3	283 (39.2), 363 (38.2), 452 (14.5)	505 (*c*; 0.16)	446, 593 (*e*)	*e*
Pt-4	371 (209.6), 481 (20.9)	415 (*c*; −), 609 (235; 0.086)	560, 607 (24.0)	530 (54.6, 27.6, 0.008)
Pt-5	338 (131.2), 382 (127.6), 485 (14.8)	498 (*c*; −), 605 (820; 0.044)	450, 558, 590 (179.0), 643	450 (14.3, 23.8, 0.024)
Pt-6	368 (199.5), 502 (16.9)	416 (*c*; −), 649 (88; 0.023)	568 (15.5), 611	535 (8.2, 21.8, 0.04)
Pt-7	352 (92.9), 487 (8.5)	464 (*c*; −)	614 (2.5)	*e*
Pt-8	286 (63.5), 386 (171.9), 468 (52.1)	416 (*c*; −), 637 (60; 0.011)	588 (13.0)	*e*

[a]Electronic absorption band maxima and molar extinction coefficients in CH_2Cl_2 at room temperature. [b]Room temperature emission band maxima and decay lifetimes measured in CH_2Cl_2 at a concentration of 1×10^{-5} mol/L. An aqueous solution of quinine sulfate (Φ_{em} = 0.546, excited at 365 nm) was used as the reference for **L-1−L-3**, **Zn-1−Zn-3**, and **Pt-1−Pt-3**. A degassed aqueous solution of $[Ru(bpy)_3]Cl_2$ (Φ_{em} = 0.042, excited at 436 nm) was used as the reference for **Pt-4−Pt-8**. [c]Too short to be measured. [d]In MTHF at a concentration of 1×10^{-5} mol/L. [e]Too weak to be measured. [f]ns TA band maximum, triplet extinction coefficient, triplet excited-state lifetime, and quantum yield measured in CH_3CN. SiNc in C_6H_6 was used as the reference (ε_{590} = 70,000 L·mol^{-1}·cm^{-1}, Φ_T = 0.20).

the Zn(II) ion decreases the electron density on the bipyridine component, resulting in increased electron-withdrawing ability of the bpy component. Consequently, the ^{1}ILCT transition from the benzothiazolylfluorenyl component to the bpy component is enhanced. The ^{1}ILCT transition becomes more salient in **Zn-3** that bears the electron-donating NPh_2 substituents. As shown in Figure 1b, the intense absorption band at 387 nm in **L-3** is split into two bands at 374 and 438 nm in **Zn-3**, with each of them possessing approximately half of the intensity of the 387 nm band in **L-3**. These two bands can be assigned to ligand $^1\pi,\pi^*$ and ^{1}ILCT transitions, respectively. Increased electron-withdrawing ability of the bpy component after complexation with Zn(II) ion red-shifts the ^{1}ILCT transition that was mixed with the $^1\pi,\pi^*$ transition in ligand **L-3**.

In comparison to the absorption spectra of **L-1−L-3** and **Zn-1−Zn-3**, the major absorption bands of **Pt-1−Pt-3** become much broader and red-shifted. In addition to the $^1\pi,\pi^*$ and ^{1}ILCT transitions that occur at the energies similar to those in their respective Zn complexes, **Pt-1** and **Pt-2** show a new peak at 417 and 430 nm, respectively, which should emanate from the metal-to-ligand charge transfer (^{1}MLCT, dπ(Pt) → π^*(bpy)) transition that is typical for Pt(II) complexes.[1−8,10−15,17−19,21,26,47] The unusually large molar extinction coefficients of this band (i.e. $\varepsilon_{417\ nm}$ = 46,900 L·mol^{-1}·cm^{-1} for **Pt-1** and $\varepsilon_{430\ nm}$ = 57,300 L·mol^{-1}·cm^{-1} for **Pt-2**) should be due to the overlap of the ^{1}MLCT transition with the ^{1}ILCT transition. For **Pt-3**, the appearance of the ^{1}MLCT band is not as obvious as those in **Pt-1** and **Pt-2**. However, the further red-shift of the low-energy absorption band implies the occurrence of ^{1}MLCT transition. This transition is likely to be in very close proximity to the ^{1}ILCT transition energetically; thus, no obvious new peak can be observed in **Pt-3**. The presence of the ^{1}MLCT transition in Pt(II) chloride complexes has been reported by McMillin and co-workers for Pt(II) terpyridyl chloride complexes[47a] and by Che and co-workers for a series of $Pt(bpy)Cl_2$ complexes.[10b] The assignment of ^{1}MLCT transition for **Pt-1−Pt-3** above 400 nm can be supported by the negative solvatochromic effect, namely the bathochromic shift of the absorption band in solvents with lower polarity (i.e., toluene) compared to those in solvents with higher polarity (i.e., MeOH), which is demonstrated in Figures S7−S9 of the Supporting Information (SI) and is a typical feature for ^{1}MLCT transition.[17,18,21,26,47] Because the ^{1}MLCT state has a smaller dipole moment than that of the ground state, less polar solvents stabilize the ^{1}MLCT excited state better than the ground state. Consequently the energy gap between the ground state and the ^{1}MLCT state decreases, and a bathochromic shift occurs in less polar solvents. In addition, similar to the trend observed from **L-1** and **L-2**, as well as **Zn-1** and **Zn-2**, each of the corresponding absorption bands in **Pt-2** is bathochromically shifted with respect to those in **Pt-1**, reflecting the effect of extended π-conjugation in the bpy ligand. It appears that the major effect of the electron-donating substituent NPh_2 vs electron-withdrawing benzothiazolyl (BTZ) substituent is the red-shifted and enhanced ^{1}ILCT transition in **L-3**, **Zn-3**, and **Pt-3** in comparison to those in **L-1**, **L-2**, **Zn-1**, **Zn-2**, **Pt-1**, and **Pt-2**.

For **Pt-4−Pt-8** that contain the acetylide ligands, the intense absorption bands (Figure 1d) below 410 nm can be assigned to predominantly $^1\pi,\pi^*$ transitions localized on either the bipyridyl or the acetylide ligands; while the broad low-energy absorption bands between 420 and 575 nm could be attributed to essentially ^{1}MLCT (dπ(Pt) → π^*(bpy))/^{1}LLCT (π(ethynylfluorene) → π^*(bpy)) transitions for **Pt-4−Pt-7**, possibly mixed with some ^{1}ILCT (π(R-fluorene) → π^*(bpy) within the bpy-based ligand for **Pt-4−Pt-7** and additional π(ethynylfluorene) → π^*(NI) for **Pt-5** within the acetylide ligands) transition(s), and predominantly ^{1}ILCT (π(NPh_2-fluorene) → π^*(bpy) within the bpy-based ligand) transition admixing with minor ^{1}MLCT (dπ(Pt) → π^*(bpy))/^{1}LLCT (π(ethynylfluorene) → π^*(bpy)) characters for **Pt-8**. These assignments are based on the comparison of the UV−vis absorption bands of these complexes to those of their corresponding Pt(II) chloride complexes **Pt-1−Pt-3**, and to those of their corresponding Pt(II) acetylide complexes without the R-fluorenyl components on the bipyridyl ligand,[21,23] as well as the minor solvatochromic effect arising from the reduced

dx.doi.org/10.1021/ic500646r | Inorg. Chem. 2014, 53, 9516−9530

dipole moments of these molecules due to the opposite direction of the dipole moments for the ^{1}MLCT/^{1}LLCT transitions and the ^{1}ILCT transitions (see Figures S10−S14 in SI), and the time-dependent density functional theory (TDDFT) calculations being discussed in the next section.

The influence of the different terminal substituents on the acetylide ligands can be evaluated by comparison of the absorption spectra of **Pt-4** and **Pt-5**, as well as **Pt-6** and **Pt-7**, respectively. Figure 1d clearly shows that the major absorption bands between 350 and 425 nm are much less intense in **Pt-5** and **Pt-7** than those in **Pt-4** and **Pt-6**, respectively, which could be explained by the less π-conjugation of the naphthalimide (NI) motif and the NPh_2 substituent with the fluorenyl motif due to the distortion of the NI and NPh_2 groups from the fluorene plane to reduce the steric hindrance. This difference also supports our assignment of the major absorption bands being dominated by the $^1\pi,\pi^*$ transitions localized on the acetylide ligands or the bipyridine ligand. The effect of extending the π-conjugation of the bipyridine ligand can be evaluated from the spectrum of **Pt-6** with respect to that of **Pt-4**, both of them possessing the same acetylide ligands but with different degrees of π-conjugation in their bipyridine ligands. As shown in Figure 2, the shoulder above 400 nm becomes

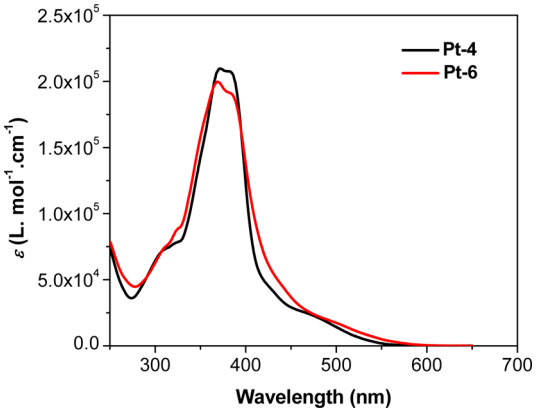

Figure 2. Comparison of UV−vis absorption spectra of **Pt-4** and **Pt-6** in CH_2Cl_2.

stronger and broader in **Pt-6** compared to that in **Pt-4**, owing to the stabilized bpy-based LUMO due to extended π-conjugation. The effect of the different positions of substituent on the bipyridine or acetylide ligands can be seen from the spectral feature of **Pt-7** and **Pt-8**. When strong electron-donating substituent NPh_2 is attached to the bipyridine ligand and the BTZ substituent is on the acetylide ligands, the UV−vis absorption of **Pt-8** becomes much stronger and broader than that of **Pt-7**. The stronger absorption between 325 and 425 nm arises from the better conjugated BTZ-fluorenylacetylide ligands, while the broader tail between 425 and 575 nm in **Pt-8** should be ascribed to the ^{1}ILCT from the diphenylamino-fluorenyl motif to the bipyridine motif in the bpy-based ligand, which appears at essentially the same position as that in **Pt-3** that has the same bpy-based ligand.

DFT Calculations. Density functional theory (DFT) calculations were carried out in CH_2Cl_2 for **Pt-4**−**Pt-8** to help us better understand the nature of the ground and low-lying singlet excited states. The ground-state electron density distribution of the five highest occupied molecular orbitals (HOMOs) and five lowest unoccupied molecular orbitals (LUMOs) of **Pt-4**−**Pt-8** are illustrated in Table 2. The results indicate that the LUMO is almost exclusively π^*(bipyridine) based for all complexes, with minor contribution from the attached fluorene or the C≡C triple bond. While the compositions of the HOMO vary for these complexes, the HOMO is primarily delocalized on both of the acetylide ligands in **Pt-4**−**Pt-6** but exclusively on one of the acetylide ligands in **Pt-7**, while the HOMO of **Pt-8** is on one of the diphenylaminofluorenyl components on the bpy ligand.

On the basis of the optimization of the ground-state geometry of the complexes, time-dependent DFT (TDDFT) calculations were performed to evaluate the nature of the major electronic transitions for complexes **Pt-4**−**Pt-8** in CH_2Cl_2. Figure 3 presents the calculated absorption spectra, and Table 3 lists the essential parameters of several low-lying electronic states obtained at the PBE1PBE level of theory. The calculation results show that electronic transition involving the HOMO → LUMO orbital pair is the dominant contributing configuration to the first singlet excited state, which occurs at 521 nm for **Pt-4**, 551 nm for **Pt-5**, 563 nm for **Pt-6**, 620 nm for **Pt-7**, and 553 nm for **Pt-8**; while transition involving the HOMO−1 → LUMO orbital pair is the dominant contributing configuration to the second singlet excited state, which appears at 491 nm for **Pt-4**, 510 nm for **Pt-5**, 530 nm for **Pt-6**, 607 nm for **Pt-7**, and 536 nm for **Pt-8**. According to the electron density distributions of the HOMO, HOMO−1, and LUMO, the lowest-energy absorption bands for these complexes should arise from the ^{1}LLCT (π(ethynylfluorene) → π^*(bpy))/^{1}MLCT (dπ(Pt) → π^*(bpy)) transitions for **Pt-4**−**Pt-7**, and ^{1}ILCT (π(NPh_2-fluorene) → π^*(bpy) within the bpy-based ligand) for **Pt-8**. The trend of the calculated lowest-energy transition is consistent with the trend of the lowest-energy absorption bands in the experimental UV−vis absorption spectra of these complexes, which supports our aforementioned assignments for the electronic transition of the lowest-energy absorption band in these complexes. In addition, for complex **Pt-8**, the ^{1}ILCT transitions (553 nm (HOMO → LUMO) and 536 nm (HOMO−1 → LUMO)) are pronouncedly red-shifted compared to those in the other complexes (i.e., 419 nm (HOMO−2 → LUMO, π(BTZ-fluorene) → π^*(bpy)) for **Pt-4**, 475 nm (HOMO → LUMO +1, π(ethynylfluorene) → π^*(NI)) for **Pt-5**, 448 nm (HOMO−2 → LUMO, π(BTZ-fluorene) → π^*(bpy)) for **Pt-6**, and 454 nm (HOMO−4 → LUMO, π(BTZ-fluorene) → π^*(bpy)) for **Pt-7**) due to the strong electron-donating ability of NPh_2 on the fluorenylbipyridine ligand. Therefore, the charge transfer bands of **Pt-3** and **Pt-8** observed in their UV−vis absoprtion spectra are quite different from those of the other complexes due to the different natures of charge transfer transition.

Emission. The emission of ligands **L-1**−**L-3**, zinc complexes **Zn-1**−**Zn-3**, and Pt complexes **Pt-1**−**Pt-8** were investigated in different solvents at r.t. and in 2-methyltetrahydrofuran (MTHF) glassy matrix at 77 K. The normalized emission spectra of these compounds in CH_2Cl_2 at the concentration of 1×10^{-5} mol/L are illustrated in Figure 4. Ligands **L-1** and **L-2** exhibit intense structured fluorescence between 350 and 500 nm (Figure 4a), which could be attributed to the $^1\pi,\pi^*$ state considering the short lifetime (<5 ns), the mirror image to their respective $^1\pi,\pi^*$ absorption bands, and the minor solvatochromic effect (SI Figures S15 and S16). Meanwhile, similar to its UV−vis absorption, the emission spectrum of **L-2** is slightly red-shifted compared to that of **L-1** due to the extended π-

dx.doi.org/10.1021/ic500646r | Inorg. Chem. 2014, 53, 9516−9530

Table 2. Contour Plots of the Five Highest Occupied Molecular Orbitals (HOMOs) and Five Lowest Unoccupied Molecular Orbitals (LUMOs) of Complexes Pt-4−Pt-8

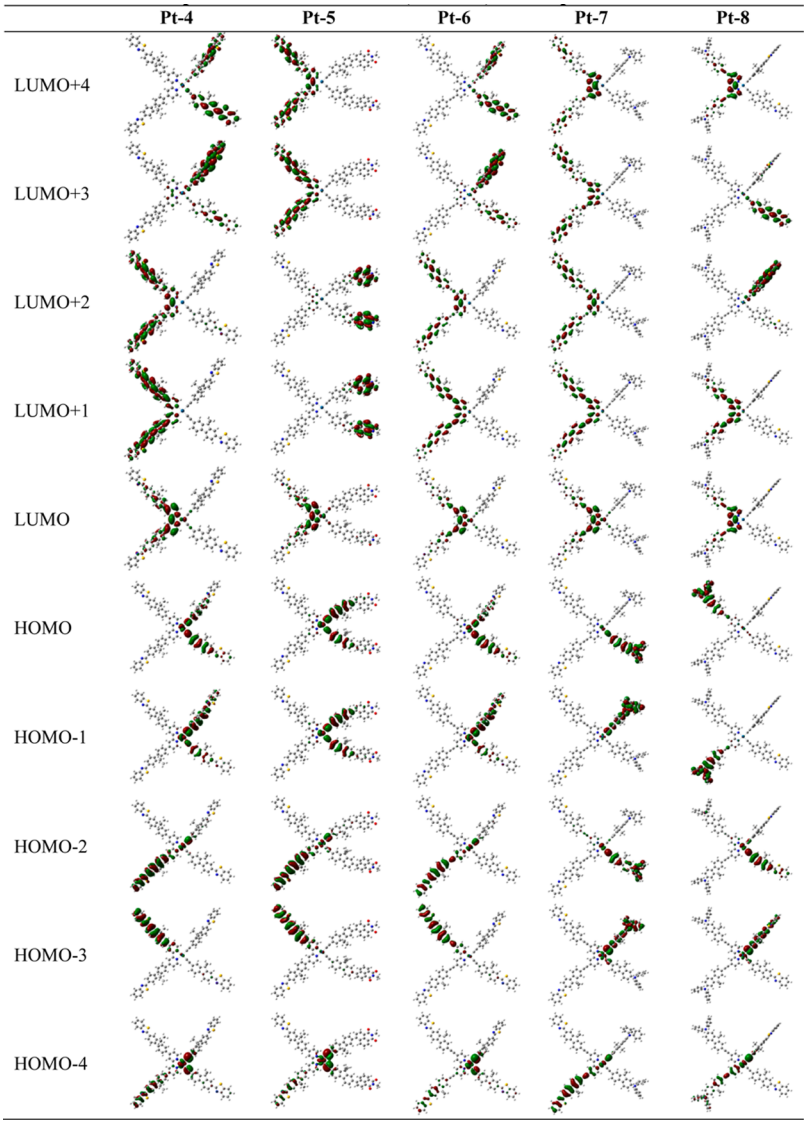

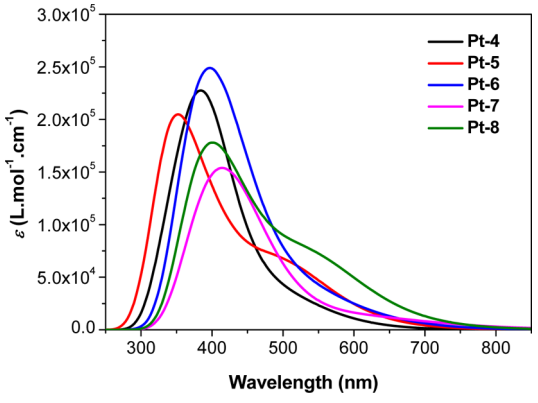

Figure 3. Calculated electronic absorption spectra of Pt complexes **Pt-4−Pt-8** in CH_2Cl_2.

conjugation from the C≡C triplet bond. In contrast, ligand **L-3** gives broad and featureless emission at ~500 nm in CH_2Cl_2, and the emission manifests a significant positive solvatochromic effect (Figure 5a). These features, along with the similar emission energy to that of **Zn-3**, suggest that the emitting state of **L-3** should be the ^{1}ILCT state from the NPh_2-fluorene component to the bipyridine component.

The emission spectra of **Zn-1−Zn-3** and **Pt-1−Pt-3** are all broad and structureless (b and c of Figure 4), and the emission energies of the zinc complexes resemble those of their corresponding Pt complexes. In addition, the emission energies of **Zn-1**/**Pt-1** and **Zn-2**/**Pt-2** are much lower than those of their corresponding ligands **L-1** and **L-2**; while the emission energies of **Zn-3**/**Pt-3** are similar to that of **L-3**. Considering the fact that the electron-withdrawing ability of the bipyridine unit increases after coordination with Zn(II) or Pt(II), the observed emission from **Zn-1−Zn-3** and **Pt-1−Pt-3** should be ascribed to fluorescence originated from the ^{1}ILCT (π(R-fluorene) → π^*(bpy)) states. Compared to **Zn-1** and **Pt-1**, **Zn-2** and **Pt-2** exhibit a more red-shifted emission band because the triple bond connection facilitates the charge transfer from the BTZ-fluorene motif to the bipyridine motif. Furthermore, the complexes bearing an electron-donating substituent on the ligand (**Zn-3**/**Pt-3**) exhibit slightly more red-shifted emission band than those bearing electron-withdrawing groups (BTZ),

dx.doi.org/10.1021/ic500646r | Inorg. Chem. 2014, 53, 9516−9530

Table 3. Excitation Energies (eV), Wavelengths (nm), Oscillator Strengths, Dominant Contributing Configurations, and the Associated Configuration Coefficients of 10 Low-Lying Electronic States of Complexes Pt-4–Pt-8 Obtained at the PBE1PBE Level of Theory

		excitation energy				
	S_n	eV	nm	f	active orbital pair of dominant configuration	configuration coefficient
Pt-4	1	2.38	521	0.2358	HOMO → LUMO	0.69
	2	2.52	491	0.4921	HOMO−1 → LUMO	0.68
	3	2.96	419	0.5095	HOMO−2 → LUMO	0.49
	4	3.07	404	0.7179	HOMO → LUMO+1	0.65
	5	3.13	396	0.0385	HOMO−7 → LUMO	0.67
	6	3.15	394	1.2437	HOMO → LUMO+3	0.46
	7	3.17	391	0.4083	HOMO−1 → LUMO+1	0.45
	8	3.21	386	0.8142	HOMO−3 → LUMO	0.46
	9	3.24	383	0.9371	HOMO−4→ LUMO	0.36
	10	3.26	381	0.0575	HOMO → LUMO+2	0.56
Pt-5	1	2.25	551	0.1638	HOMO → LUMO	0.69
	2	2.43	510	0.9085	HOMO−1 → LUMO	0.68
	3	2.59	480	0.1130	HOMO → LUMO+2	0.62
	4	2.61	475	0.3300	HOMO → LUMO+1	0.61
	5	2.80	443	0.0480	HOMO−1 → LUMO+1	0.50
					HOMO−1 → LUMO+2	0.37
	6	2.81	441	0.0349	HOMO−1 → LUMO+2	0.52
	7	2.88	431	0.0797	HOMO−4 → LUMO	0.57
	8	2.98	416	0.2406	HOMO → LUMO+3	0.68
	9	3.08	402	0.7832	HOMO−1 → LUMO+3	0.56
					HOMO−3→ LUMO	0.21
	10	3.15	394	0.3171	HOMO → LUMO+4	0.35
					HOMO−2 → LUMO	0.30
					HOMO−1→ LUMO+3	0.29
Pt-6	1	2.20	563	0.2750	HOMO → LUMO	0.69
	2	2.34	530	0.4826	HOMO−1 → LUMO	0.68
	3	2.77	448	0.7559	HOMO−2 → LUMO	0.52
	4	2.84	437	0.7875	HOMO → LUMO+1	0.65
	5	2.92	425	0.9621	HOMO−1 → LUMO+1	0.45
	6	2.97	417	0.1922	HOMO−1 → LUMO+1	0.49
	7	2.98	416	0.0213	HOMO−7 → LUMO	0.67
	8	3.04	407	0.6952	HOMO−4 → LUMO	0.45
	9	3.15	394	0.6910	HOMO → LUMO+2	0.44
	10	3.18	391	0.7451	HOMO → LUMO+2	0.42
Pt-7	1	2.00	620	0.2680	HOMO → LUMO	0.67
	2	2.04	607	0.0001	HOMO−1 → LUMO	0.68
	3	2.54	488	0.0435	HOMO−2 → LUMO	0.60
	4	2.55	485	0.2129	HOMO → LUMO+1	0.64
	5	2.59	478	0.0000	HOMO−1 → LUMO+1	0.70
	6	2.63	472	0.0036	HOMO−3 → LUMO	0.65
	7	2.73	454	1.1763	HOMO−4 → LUMO	0.59
	8	2.90	428	0.0531	HOMO → LUMO+2	0.67
	9	2.94	422	0.0003	HOMO−1 → LUMO+2	0.68
	10	2.95	420	0.9798	HOMO−5 → LUMO	0.52
Pt-8	1	2.24	553	0.8297	HOMO → LUMO	0.50
	2	2.31	536	0.6460	HOMO−1 → LUMO	0.68
	3	2.36	524	0.0975	HOMO−2 → LUMO	0.44
	4	2.41	515	0.0028	HOMO−3 → LUMO	0.60
	5	2.84	436	0.7403	HOMO−4 → LUMO	0.59
	6	2.85	435	0.9171	HOMO → LUMO+1	0.59
	7	2.88	430	0.4708	HOMO−1 → LUMO+1	0.59
	8	3.01	411	0.0025	HOMO−9 → LUMO+1	0.68
	9	3.03	409	0.1527	HOMO−2 → LUMO+1	0.65
	10	3.12	397	0.0260	HOMO−3 → LUMO+1	0.68

i.e. **Zn-2** and **Pt-2**. The strong electron-donating substituent on the ligand of **Zn-3**/**Pt-3** also makes the emission of these two complexes very sensitive to the polarity of the solvents. As shown in Figure 5b and SI Figure S19, the emission of **Pt-3** and **Zn-3** exhibits salient positive solvatochromic effect due to the stronger intraligand charge transfer (^{1}ILCT).

For the Pt acetylide complexes **Pt-4**–**Pt-8**, excitation at their respective absorption band maxima (365–395 nm) at room temperature results in two groups of luminescence bands except for complex **Pt-7** (Figure 4d). The high-energy emission bands (i.e., below 550 nm) of these complexes are all short-lived (<5 ns) and insensitive to oxygen quenching and thus are considered as fluorescence. However, the nature of the

dx.doi.org/10.1021/ic500646r | Inorg. Chem. 2014, 53, 9516–9530

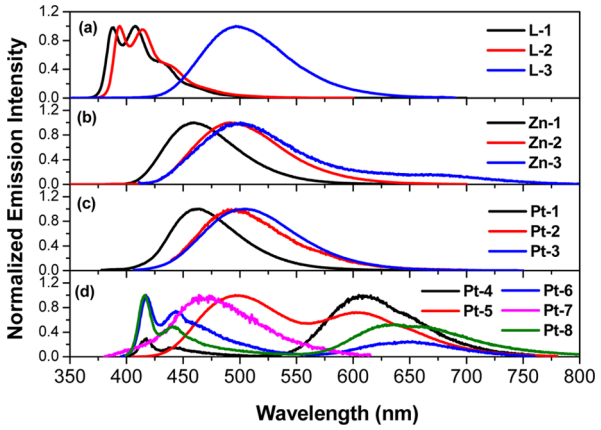

Figure 4. Normalized emission spectra of (a) ligands **L-1** (λ_{ex} = 355 nm), **L-2** (λ_{ex} = 301 nm), and **L-3** (λ_{ex} = 305 nm) in CH_2Cl_2 ($c = 1 \times 10^{-5}$ mol/L); (b) complexes **Zn-1** (λ_{ex} = 372 nm), **Zn-2** (λ_{ex} = 380 nm), and **Zn-3** (λ_{ex} = 396 nm) in CH_2Cl_2 ($c = 1 \times 10^{-5}$ mol/L); (c) complexes **Pt-1** (λ_{ex} = 368 nm), **Pt-2** (λ_{ex} = 398 nm), and **Pt-3** (λ_{ex} = 395 nm) in CH_2Cl_2 ($c = 1 \times 10^{-5}$ mol/L); (d) complexes **Pt-4** (λ_{ex} = 385 nm), **Pt-5** (λ_{ex} = 395 nm), **Pt-6** (λ_{ex} = 385 nm), **Pt-7** (λ_{ex} = 365 nm) and **Pt-8** (λ_{ex} = 388 nm) in CH_2Cl_2 ($c = 1 \times 10^{-5}$ mol/L).

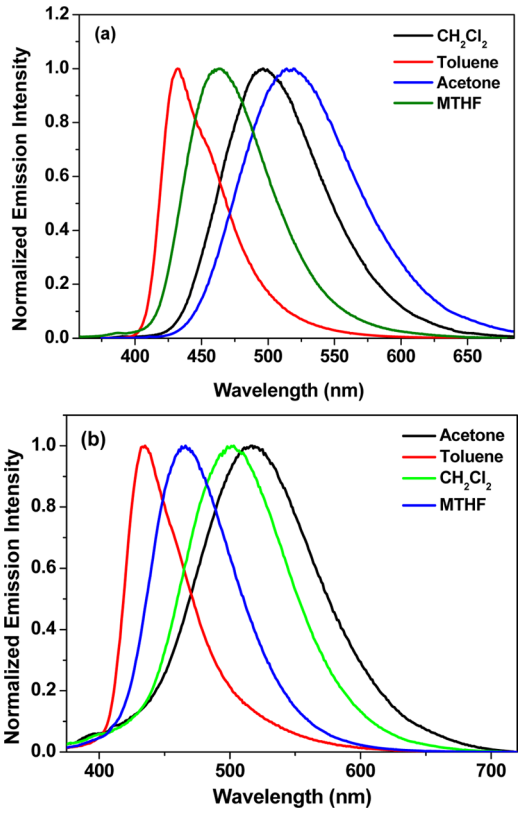

Figure 5. Normalized emission spectra of (a) **L-3** and (b) **Pt-3** in different solvents at room temperature. λ_{ex} = 365 nm and A_{365} = 0.08 in a 1 cm cuvette.

fluorescence is different for these complexes. For **Pt-4**, **Pt-6**, and **Pt-8**, the high-energy structured emission is assigned to fluorescence from the $^1\pi,\pi^*$ state of the acetylide ligand in view of the same shape and energy of these emission bands in these complexes (which implies that the emission originates from the same structural component) and the emission energy similar to that reported for the benzothiazolylfluorenylacetylide ligand.[25] For **Pt-5**, the high-energy structureless emission band could be tentatively attributed to the ^{1}ILCT state from the ethynylfluorenyl component of the acetylide ligand to the naphthalimide component. This assignment can be partially supported by the similar shape and energy of this band to those of the emission from the Pt(II) complex with the same acetylide ligand.[23] The weak featureless emission from **Pt-7** likely emanates from the ^{1}LLCT state associated with the transition from the diphenylaminofluorenyl component to the bipyridine component, considering its distinct feature from the other complexes and the nature of the lowest singlet excited state.

In contrast to the high-energy emission band, the low-energy emission bands of **Pt-4**–**Pt-6** and **Pt-8** all exhibit drastic red-shifts with respect to their lowest-energy absorption bands and the excitation wavelengths; they are readily quenched by oxygen; and the lifetimes in degassed CH_2Cl_2 solutions vary from tens to hundreds of nanoseconds. Considering all these facts, we believe that the low-energy emission is phosphorescence from the T_1 state. The structureless feature of these bands suggest the charge transfer nature of the emitting states. With reference to the related Pt(II) diimine acetylide complexes, the emitting state could be tentatively assigned to the ^{3}MLCT/^{3}LLCT states for **Pt-4**, **Pt-6**, and **Pt-8**,[6,15,17−19,21,22,24,25] and to the predominantly ^{3}ILCT (π-(ethynylfluorene) → π^*(NI)) state for **Pt-5**.[23] Attribution of the triplet emitting state of **Pt-5** predominantly to the ^{3}ILCT state rather than the naphthalimide-localized $^3\pi,\pi^*$ state is based on the following facts: (1) the low-energy emission band observed from **Pt-5** is structureless and relatively short-lived (~820 ns in CH_2Cl_2), while the naphthalimide-localized $^3\pi,\pi^*$ emission possesses a clear vibronic structure and a much longer lifetime (124 μs in MTHF);[14] (2) the thermally induced Stokes shifts (ΔE_S) for **Pt-5** is approximately 1390 cm^{-1}, which is remarkably different from the extremely small ΔE_S for the naphthalimide-localized $^3\pi,\pi^*$ emission (131 cm^{-1} in MTHF),[14] implying the charge transfer nature of the emitting state for **Pt-5**; (3) both the shape and the energy of the 605 nm emission band of **Pt-5** resemble those of the corresponding Pt(II) complex with the same naphthalimide-substituted fluorenylacetylide ligands but without the benzothiazolylfluorenyl substituents on the bipyridyl ligand, of which the emitting state is ascribed to the ^{3}ILCT/^{3}MLCT/^{3}LLCT excited states.[23] Extended π-conjugation of the bipyridyl ligand causes a red-shift of the phosphorescence band in **Pt-6** compared to that in **Pt-4**, while the naphthalimide substituent on the acetylide ligands changes the nature of the emitting state and raises the phosphorescence energy in **Pt-5** with respect to that of **Pt-4**. In contrast, a strong electron-donating substituent (NPh_2) on the acetylide ligands quenches the phosphorescence of **Pt-7**.

The different origins of the dual emission of complexes **Pt-4**–**Pt-6** and **Pt-8** can be partially supported by the difference in their excitation spectra monitored at the high-energy and low-energy emission bands, respectively. As examplified in Figure 6 for **Pt-5** and **Pt-8**, the excitation spectra exhibit a broad tail above 425 nm (which corresponds to the charge transfer tail in their respective UV–vis absorption spectra) when monitored at their respective low-energy emission bands in comparison to those monitored at the respective high-energy emission bands (which only exhibit a band below ~425 nm that corresponds to the major absorption bands in their corresponding UV–vis absorption spectra). This implies that the low-energy emission band should emanate from the charge transfer excited state.

dx.doi.org/10.1021/ic500646r | Inorg. Chem. 2014, 53, 9516−9530

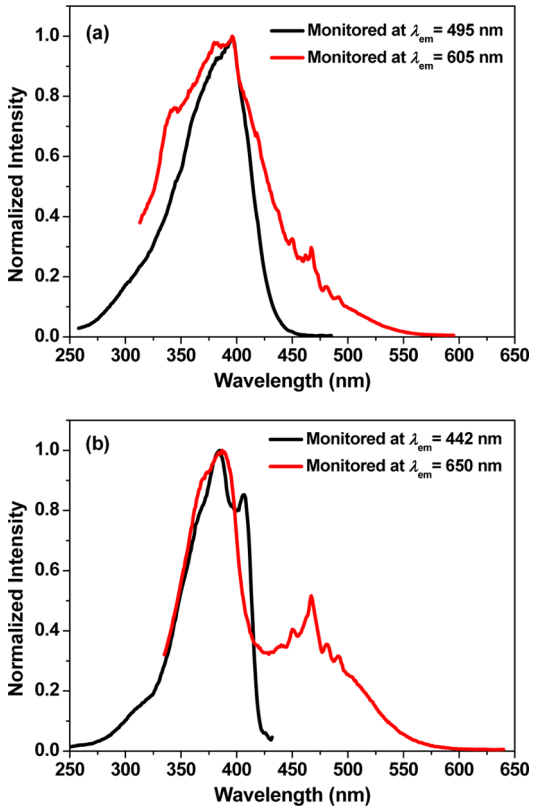

Figure 6. Normalized excitation spectra of (a) **Pt-5** and (b) **Pt-8** in CH_2Cl_2 monitored at different emission wavelengths. $c = 2 \times 10^{-6}$ mol/L.

The similar phenomenon was observed for **Pt-4** and **Pt-6**. Although the dual emission is not very common in heavy-metal-containing organometallic complexes, this phenomenon has been reported for other heavy-metal -containing organometallic complexes, including some Pt(II) complexes.[25,47a,b,48] The observation of dual emission in **Pt-4**−**Pt-6** and **Pt-8** should be attributed to the increased π-conjugation of the bipyridyl ligand, which decreases the spin−orbit coupling in the Pt(II) complex due to smaller contribution of Pt-centered orbitals to the frontier molecular orbitals.[48i] As a result, the intersystem crossing in these complexes becomes inefficient, which is confirmed by the much smaller triplet quantum yields of these complexes (listed in Table 1) that are measured by the transient absorption measurement.

The solvent-dependent emission of **Pt-4**−**Pt-8** was investigated and the results are presented in the SI Figures S22−S26 and in Table S1. Although the solvatochromic effect of **Pt-4**−**Pt-8** is minor, the coordinating solvent-induced quenching is clearly evident for **Pt-4**, **Pt-6**, and **Pt-8**, implying the involvement of ^{3}MLCT character in the emission. In contrast, no quenching was observed in CH_3CN for complex **Pt-5**, which is consistent with the ^{3}ILCT assignment for **Pt-5**.

The emission of the ligands **L-1**−**L-3**, the zinc complexes **Zn-1**−**Zn-3**, and the Pt complexes **Pt-1**−**Pt-8** was also studied in MTHF glassy matrix at 77 K to understand the nature of the emitting state at low temperature. The emission band maxima and lifetimes are listed in Table 1, and the spectra are presented in the SI Figures S27−S40. The emission spectra of **L-1**−**L-3** become narrower at 77 K glassy matrix, while the emission spectra of **Zn-1**−**Zn-3** are structured and blue-shifted at 77 K. All these phenomena arise from the rigidochromic effect,[49] and the emission is attributed to fluorescence from the same singlet excited states that give rise to the room temperature fluorescence. For **Pt-1** and **Pt-2**, the 77 K emission is much red-shifted and clearly structured (the vibronic spacing is 1319 cm^{-1} for **Pt-1** and 1253 cm^{-1} for **Pt-2**) in comparison to their respective fluorescence at room temperature, which should be assigned to phosphorescence either from the $^3\pi,\pi^*$ state of the ligand or the ^{3}MLCT state of the complex. Similar to their room temperature fluorescence, the energy of the 77 K phosphorescence of **Pt-2** is also substantially reduced with respect to that of **Pt-1**, reflecting the effect of the extended π-conjugation in the ligand. For **Pt-3**, dual emission was detected at 77 K as demonstrated in SI Figure S35. The high-energy structureless emission band is attributed to the ^{1}ILCT fluorescence, while the low-energy emission could be tentatively ascribed to ^{3}ILCT phosphorescence. However, due to the very weak phosphorescence signal, the lifetimes of the phosphorescence of **Pt-1**−**Pt-3** could not be measured. Thus, the nature of the emitting state at 77 K could not be exclusively attributed.

For complexes **Pt-4**−**Pt-6** and **Pt-8**, except for **Pt-5** that exhibits dual emission at 77 K, the emission spectra of the other three complexes at 77 K all become narrower, structured, and blue-shifted in comparison to their respective phosphorescence band at room temperature. The thermally induced Stokes shifts (ΔE_s) for **Pt-4**−**Pt-6** and **Pt-8** are between 1308 and 2197 cm^{-1}. These large ΔE_S values imply a significant dipole moment change between the ground and the excited states, which is commonly seen for charge transfer excited states. Therefore, the emitting states for these complexes at 77 K can be tentatively attributed to the ^{3}MLCT/^{3}LLCT states for **Pt-4**, **Pt-6**, and **Pt-8**, and predominantly ^{3}ILCT state for **Pt-5**, similar to those attributed to these complexes at r.t. In contrast, the emission band at 77 K for **Pt-7** is drastically red-shifted and long-lived in comparison to that at r.t. (see Figure S39 of the SI and Table 1). This indicates that the observed emission at 77 K for **Pt-7** is phosphorescence. Considering our attribution of the emitting state at r.t. to ^{1}LLCT for **Pt-7**, we tentatively assign the emitting state at 77 K to the ^{3}LLCT state for **Pt-7**.

Triplet Transient Absorption. One of the potential applications of the Pt(II) diimine complexes is as nonlinear absorbing materials, which is closely related to the excited-state absorption. To understand the excited-state absorption of the Pt(II) complexes in this work, nanosecond transient difference absorption spectra (TA) of **Pt-1**−**Pt-8** were measured. The shape of the TA spectrum provides us information on the spectral region where the triplet excited state absorbs more strongly than the ground state, and the decay of the TA can help us to understand the decay characteristics of the triplet excited state. To better understand the nature of the triplet excited state that gives rise to the observed TA, the TA characteristics of the corresponding ligands and the zinc complexes were studied as well. The time-resolved nanosecond transient difference absorption (TA) spectra of **L-1**, **L-2**, **Zn-1**, **Zn-2**, **Pt-1**, **Pt-2**, **Pt-4**, **Pt-5**, **Pt-6**, and **Pt-8** in CH_3CN are presented in Figure 7, and the triplet excited-state lifetimes deduced from the TA decay profiles are listed in Table 1. The transient absorption of **L-3**, **Zn-3**, **Pt-3**, and **Pt-7** (all of these contain electron-donating NPh_2 substituent on their ligands) was too weak to be measured due to their short-lived triplet excited states.

As shown in Figure 7, the spectral features of **L-1** and **Zn-1** resemble each other, both showing a single long-lived TA band

dx.doi.org/10.1021/ic500646r | Inorg. Chem. 2014, 53, 9516−9530

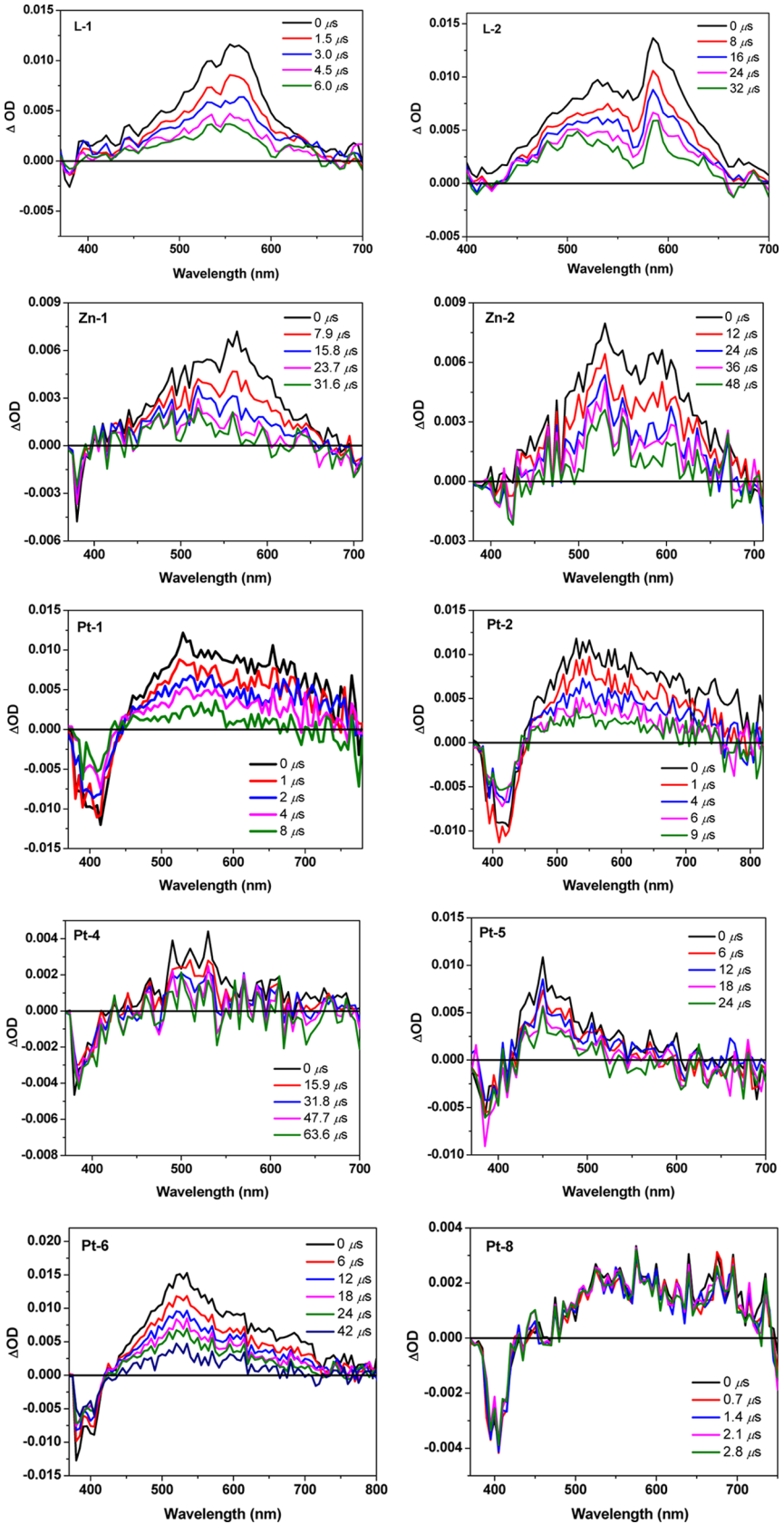

Figure 7. Time-resolved nanosecond transient difference absorption spectra of **L-1**, **L-2**, **Zn-1**, **Zn-2**, **Pt-1**, **Pt-2**, **Pt-4**, **Pt-5**, **Pt-6**, and **Pt-8** in CH_3CN solution. λ_{ex} = 355 nm. A_{355} = 0.4 in a 1 cm cuvette.

at ~550 nm. For **L-2** and **Zn-2**, the TA spectra appear as two overlapped bands at ~525 and 600 nm, and the lifetimes are much longer than those of **L-1** and **Zn-1**. Considering the shape of the spectrum and the long lifetime, we tentatively

dx.doi.org/10.1021/ic500646r | Inorg. Chem. 2014, 53, 9516−9530

assign the excited state giving rise to the observed TA to $^3\pi,\pi^*$ states for **L-1**, **L-2**, **Zn-1**, and **Zn-2**. The TA spectra of **Pt-1** and **Pt-2** are similar in that they both possess a broad positive absorption band at ~530 nm and a bleaching band at 410 and 420 nm, respectively. In view of the similar absorption band maximum to that of their corresponding zinc complexes, but much broader positive absorption band and shorter lifetimes, we attribute the TA of **Pt-1** and **Pt-2** to mixed $^3\pi,\pi^*/^3$MLCT states. Complexes **Pt-4**, **Pt-5**, and **Pt-6** exhibit bleaching of the ground-state absorption below 380 nm and narrow positive absorption bands between 450 and 600 nm, while **Pt-8** shows a bleaching band at 405 nm and a broad positive absorption band between 425 and 750 nm. However, the TA signals from **Pt-4**, **Pt-5**, and **Pt-8** are very weak. The triplet lifetimes deduced from the decay of TA for **Pt-4**–**Pt-6** (see Table 1) are drastically different from those obtained from the decay of the emission (Table S1 in the SI) in CH_3CN, implying that the TA of these complexes emanates from an excited state different from the emitting state. Considering the long TA lifetimes and narrow positive absorption bands, the triplet excited states giving rise to the observed TA of these complexes can be assigned to the $^3\pi,\pi^*$ states, possibly mixed with minor ^{3}MLCT/^{3}LLCT characters. The different natures of the emitting state and the TA state have been observed in some Ru(II), Os(II), and Pt(II) complexes before.[50−52]

Reverse Saturable Absorption. The TA spectra shown in Figure 7 suggest that most of the Pt complexes studied in this work exhibit stronger triplet excited-state absorption than that of the ground state in the visible spectral region; thus, reverse saturable absorption (RSA, i.e. absorptivity increases with increased incident energy due to excited-state absorption stronger than the ground-state absorption) is anticipated to occur in the visible spectral region for these Pt(II) complexes. Nonlinear transmission experiment was carried out at 532 nm using 4.1 ns laser pulses for **Pt-1**–**Pt-8** CH_2Cl_2 solutions in a 2 mm cuvette to demonstrate the RSA. The concentration of each complex solution was adjusted to a linear transmission of 80% at 532 nm in the 2 mm cuvette for easy comparison. In such a case, the same number of molecules will be populated to the singlet excited state upon laser excitation, then the observed different degrees of RSA should arise from the difference in their excited-state absorption. Figure 8 displays the nonlinear transmission vs incident energy curves for these Pt complexes at 532 nm. When the incident energy increases, the transmission of the sample solution decreases, clearly indicating the occurrence of RSA. The strength of the RSA at 532 nm for these complexes follows this trend: **Pt-2** > **Pt-4** > **Pt-5** ≈ **Pt-1** > **Pt-7** > **Pt-6** > **Pt-3** > **Pt-8**, with **Pt-2** exhibiting the strongest RSA.

This trend clearly indicates that incorporation of electron-donating substituent NPh_2 on the bipyridyl ligand significantly decreases the RSA, as manifested by **Pt-3** and **Pt-8**, because the ground-state absorption at 532 nm is drastically increased by the enhanced intraligand charge transfer transition in these two complexes. It is known that one of the determining factors for the strength of RSA is the ratio of the excited-state absorption cross section with respect to that of the ground state (σ_{ex}/σ_0). The increased ground-state absorption at 532 nm for **Pt-3** and **Pt-8** decreases the σ_{ex}/σ_0 ratios and reduces the RSA. On the other hand, shorter π-conjugation in the bipyridyl ligand increases the RSA at 532 nm, which is evident by the RSA of **Pt-4** and **Pt-5** in comparison to those of **Pt-6** and **Pt-7**. However, the RSA of **Pt-2** (which has the same bipyridyl ligand as **Pt-6** and **Pt-7**) is much stronger than that of **Pt-1** (which has the same bipyridyl ligand as **Pt-4** and **Pt-5**). We believe that this should be due to the stronger excited-state absorption of **Pt-2** than that of **Pt-1** at 532 nm.

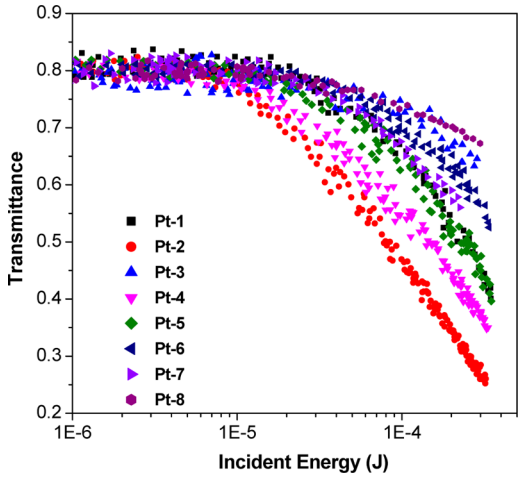

Figure 8. Nonlinear transmission curves for Pt complexes **Pt-1**–**Pt-8** in CH_2Cl_2 for 4.1 ns laser pulses at 532 nm in a 2 mm cuvette. The radius of the beam waist at the focal point was ~96 μm. The linear transmission for all sample solutions was adjusted to 80% in the 2 mm cuvette.

CONCLUSIONS

A series of Pt(II) complexes with different arylfluorenyl components on both of the acetylide and bipyridyl ligands (**Pt-4**–**Pt-8**) were synthesized, and their photophysical properties were systematically investigated. These complexes exhibit the bpy or the acetylide ligand localized $^1\pi,\pi^*$ transitions in the UV and blue spectral region, and broad, structureless ^{1}MLCT/^{1}LLCT or ^{1}ILCT absorption band in the visible spectral region. The assignment of the absorption bands is supported by comparison with their corresponding ligands, the respective zinc chloride complexes, and the respective Pt(II) chloride complexes, as well as the TDDFT calculations. All complexes are emissive at r.t. in solution and at 77 K in glassy matrix. **Pt-4**, **Pt-6**, and **Pt-8** exhibit dual emission, i.e. acetylide ligand localized $^1\pi,\pi^*$ fluorescence and ^{3}MLCT (dπ(Pt) → π^*(bpy))/^{3}LLCT (π(ethynylfluorene) → π^*(bpy)) phosphorescence, upon excitation at their respective absorption band maxima, while the emitting states of **Pt-5** are ^{1}ILCT and ^{3}ILCT (π(ethynylfluorene) → π^*(NI) in the acetylide ligand). In contrast, **Pt-7** only manifests ^{1}LLCT (π(NPh_2-fluorenylacetylide) → π^*(bpy)) fluorescence upon excitation. Obviously, the different substituents on the acetylide ligands influence the nature of the emitting states dramatically. The ns TA spectroscopic study indicates that **Pt-4**–**Pt-6** and **Pt-8** exhibit weak to moderate excited-state absorption in the visible spectral region, while the TA of **Pt-7** with electron-donating substituent NPh_2 on the acetylide ligands is too weak to be monitored because of the short-lived triplet excited state. Due to the stronger triplet excited-state absorption than the ground-state absorption at 532 nm for these complexes, moderate to strong RSA was observed at 532 nm for ns laser pulses. The strength of RSA follows this trend: **Pt-2** > **Pt-4** > **Pt-5** ≈ **Pt-1** > **Pt-7** > **Pt-6** > **Pt-3** > **Pt-8**. Incorporation of electron-donating substituent NPh_2 on the bipyridyl ligand significantly decreases the RSA, as manifested by **Pt-3** and **Pt-8**, while shorter π-

dx.doi.org/10.1021/ic500646r | Inorg. Chem. 2014, 53, 9516−9530

conjugation in the bipyridyl ligand increases the RSA at 532 nm, reflected by the RSA of **Pt-4** and **Pt-5** in comparison to those of **Pt-6** and **Pt-7**. Therefore, the substituent on either the acetylide ligands or the bipyridyl ligand affects the singlet and triplet excited state characteristics significantly, which subsequently influences the RSA.

■ ASSOCIATED CONTENT

Supporting Information

The normalized UV−vis absorption spectra and emission spectra of **L-1**−**L-3**, **Zn-1**−**Zn-3**, and **Pt-1**−**Pt-8** in different solvents; emission parameters of **L-1**−**L-3**, **Zn-1**−**Zn-3**, and **Pt-1**−**Pt-8** in different solvents; emission spectra of **L-1**−**L-3**, **Zn-1**−**Zn-3**, and **Pt-1**−**Pt-8** in MTHF glassy matrix at 77 K; time-resolved nanosecond transient difference absorption spectra of **Pt-7** in CH_3CN. This material is available free of charge via the Internet at http://pubs.acs.org.

■ AUTHOR INFORMATION

Corresponding Author

*E-mail: Wenfang.Sun@ndsu.edu; telephone: 701-231-6254; fax: 701-231-8831.

Present Address

[‖](R.L.) Department of Applied Chemistry, College of Sciences, Nanjing Tech University, Nanjing 211816, P.R. China.

Notes

The authors declare no competing financial interest.

■ ACKNOWLEDGMENTS

This work is partially supported by the National Science Foundation (CAREER CHE-0449598) and partially supported by the Army Research Laboratory (W911NF-06-2-0032).

■ REFERENCES

(1) (a) Williams, J. A. G. *Top. Curr. Chem.* **2007**, *281*, 205−268. (b) Muro, M. L.; Rachford, A. A.; Wang, X.; Castellano, F. N. *Top. Organomet. Chem.* **2010**, *29*, 159−191. (c) Castellano, F. N.; Pomestchenko, I. E.; Shikhova, E.; Hua, F.; Muro, M. L.; Rajapakse, N. *Coord. Chem. Rev.* **2006**, *250*, 1819−1828. (d) Archer, S.; Weinstein, J. A. *Coord. Chem. Rev.* **2012**, *256*, 2530−2561.

(2) Liu, Y.; Li, Q.; Zhao, J.; Guo, H. *RSC Adv.* **2012**, *2*, 1061−1067.

(3) Liu, Y.; Wu, W.; Zhao, J.; Zhang, X.; Guo, H. *Dalton Trans.* **2011**, *40*, 9085−9089.

(4) Huang, L.; Zeng, L.; Guo, H.; Wu, W.; Wu, W.; Ji, S.; Zhao, J. *Eur. J. Inorg. Chem.* **2011**, *29*, 4527−4533.

(5) Sun, H.; Guo, H.; Wu, W.; Liu, X.; Zhao, J. *Dalton Trans.* **2011**, *40*, 7834−7841.

(6) Li, Q.; Guo, H.; Ma, L.; Wu, W.; Liu, Y.; Zhao, J. *J. Mater. Chem.* **2012**, *22*, 5319−5329.

(7) Hissler, M.; McGarrah, J. E.; Connick, W. B.; Geiger, D. K.; Cummings, S. D.; Eisenberg, R. *Coord. Chem. Rev.* **2000**, *208*, 115−137.

(8) McGarrah, J. E.; Kim, Y.-J.; Hissler, M.; Eisenberg, R. *Inorg. Chem.* **2001**, *40*, 4510−4511.

(9) Suzuki, S.; Sugimura, R.; Kozaki, M.; Keyaki, K.; Nozaki, K.; Ikeda, N.; Akiyama, K.; Okada, K. *J. Am. Chem. Soc.* **2009**, *131*, 10374−10375.

(10) (a) Chan, S.-C.; Chan, M. C. W.; Wang, Y.; Che, C.-M.; Cheung, K.-K.; Zhu, N. *Chem.—Eur. J.* **2001**, *7*, 4180−4190. (b) Miskowski, V. M.; Houlding, V. H.; Che, C.-M.; Wang, Y. *Inorg. Chem.* **1993**, *32*, 2518−2524.

(11) Pomestchenko, I. E.; Castellano, F. N. *J. Phys. Chem. A* **2004**, *108*, 3485−3492.

(12) Pomestchenko, I. E.; Luman, C. R.; Hissler, M.; Ziessel, R.; Castellano, F. N. *Inorg. Chem.* **2003**, *42*, 1394−1396.

(13) Guo, H.; Ji, S.; Wu, W.; Wu, W.; Shao, J.; Zhao, J. *Analyst* **2010**, *135*, 2832−2840.

(14) Guo, H.; Muro-Small, M. L.; Ji, S.; Zhao, J.; Castellano, F. N. *Inorg. Chem.* **2010**, *49*, 6802−6804.

(15) Sun, W.; Zhang, B.; Li, Y.; Pritchett, T. M.; Li, Z.; Haley, J. E. *Chem. Mater.* **2010**, *22*, 6384−6392.

(16) Pritchett, T. M.; Sun, W.; Zhang, B.; Ferry, M. J.; Li, Y.; Haley, J. E.; Mackie, D. M.; Shensky, W., III; Mott, A. G. *Opt. Lett.* **2010**, *35*, 1305−1307.

(17) Wadas, T. J.; Lachicotte, R. J.; Eisenberg, R. *Inorg. Chem.* **2003**, *42*, 3772−3778.

(18) Hissler, M.; Connick, W. B.; Geiger, D. K.; McGarrah, J. E.; Lipa, D.; Lachicotte, R. J.; Eisenberg, R. *Inorg. Chem.* **2000**, *39*, 447−457.

(19) Whittle, C. E.; Weinstein, J. A.; George, M. W.; Schanze, K. S. *Inorg. Chem.* **2001**, *40*, 4053−4062.

(20) Haskins-Glusac, K.; Ghiviriga, I.; Abboud, K. A.; Schanze, K. S. *J. Phys. Chem. B* **2004**, *108*, 4969−4978.

(21) Liu, R.; Zhou, D.; Azenkeng, A.; Li, Z.; Li, Y.; Glusac, K. D.; Sun, W. *Chem.—Eur. J.* **2012**, *18*, 11440−11448.

(22) Li, Z.; Badaeva, E.; Zhou, D.; Bjorgaard, J.; Glusac, K. D.; Killina, S.; Sun, W. *J. Phys. Chem. A* **2012**, *116*, 4878−4889.

(23) Liu, R.; Azenkeng, A.; Li, Y.; Sun, W. *Dalton Trans.* **2012**, *41*, 12353−12357.

(24) Liu, R.; Azenkeng, A.; Zhou, D.; Li, Y.; Glusac, K. D.; Sun, W. *J. Phys. Chem. A* **2013**, *117*, 1907−1917.

(25) Li, Y.; Liu, R.; Badaeva, E.; Kilina, S.; Sun, W. *J. Phys. Chem. C* **2013**, *117*, 5908−5918.

(26) Zhang, B.; Li, Y.; Liu, R.; Pritchett, T. M.; Azenkeng, A.; Ugrinov, A.; Haley, J. E.; Li, Z.; Hoffmann, M. R.; Sun, W. *Chem.—Eur. J.* **2012**, *18*, 4593−4606.

(27) Ji, Z.; Li, Y.; Pritchett, T. M.; Makarov, N. S.; Haley, J. E.; Li, Z.; Drobizhev, M.; Rebane, A.; Sun, W. *Chem.—Eur. J.* **2011**, *17*, 2479−2491.

(28) Crosby, G. A.; Demas, J. N. *J. Phys. Chem.* **1971**, *75*, 991−1024.

(29) Van Houten, J.; Watts, R. J. *J. Am. Chem. Soc.* **1976**, *98*, 4853−4858.

(30) Melhuish, W. H. *J. Phys. Chem.* **1961**, *65*, 229−235.

(31) Carmichael, I.; Hug, G. L. *J. Phys. Chem. Ref. Data* **1986**, *15*, 1−250.

(32) Kumar, C. V.; Qin, L.; Das, P. K. *J. Chem. Soc., Faraday Trans. 2* **1984**, *80*, 783−793.

(33) Firey, P. A.; Ford, W. E.; Sounik, J. R.; Kenney, M. E.; Rodgers, M. A. J. *J. Am. Chem. Soc.* **1988**, *110*, 7626−7630.

(34) Perdew, J. P.; Burke, K.; Ernzerhof, M. *Phys. Rev. Lett.* **1996**, *77*, 3865−3868.

(35) Ernzerhof, M.; Scuseria, G. E. *J. Chem. Phys.* **1999**, *110*, 5029−5036.

(36) Adamo, C.; Barone, V. *J. Chem. Phys.* **1999**, *110*, 6158−6170.

(37) Clark, T.; Chandrasekhar, J.; Spitznagel, G. W.; Schleyer, P. V. R. *J. Comput. Chem.* **1983**, *4*, 294−301.

(38) Francl, M. M.; Pietro, W. J.; Hehre, W. J.; Binkley, J. S.; Gordon, M. S.; DeFrees, D. J.; Pople, J. A. *J. Chem. Phys.* **1982**, *77*, 3654−3665.

(39) Gill, P. M. W.; Johnson, B. G.; Pople, J. A.; Frisch, M. J. *Chem. Phys. Lett.* **1992**, *197*, 499−505.

(40) Hariharan, P. C.; Pople, J. A. *Theor. Chim. Acta* **1973**, *28*, 213−222.

(41) Krishnan, R.; Binkley, J. S.; Seeger, R.; Pople, J. A. *J. Chem. Phys.* **1980**, *72*, 650−654.

(42) Hay, P. J.; Wadt, W. R. *J. Chem. Phys.* **1985**, *82*, 299−310.

(43) Hay, P. J.; Wadt, W. R. *J. Chem. Phys.* **1985**, *82*, 270−283.

(44) Wadt, W. R.; Hay, P. J. *J. Chem. Phys.* **1985**, *82*, 284−298.

(45) Frisch, M. J.; Trucks, G. W.; Schlegel, H. B.; Scuseria, G. E.; Robb, M. A.; Cheeseman, J. R.; Scalmani, G.; Barone, V.; Mennucci, B.; Petersson, G. A.; Nakatsuji, H.; Caricato, M.; Li, X.; Hratchian, H. P.; Izmaylov, A. F.; Bloino, J.; Zheng, G.; Sonnenberg, J. L.; Hada, M.; Ehara, M.; Toyota, K.; Fukuda, R.; Hasegawa, J.; Ishida, M.; Nakajima, T.; Honda, Y.; Kitao, O.; Nakai, H.; Vreven, T.; Montgomery, J. A., Jr.; Peralta, J. E.; Ogliaro, F.; Bearpark, M.; Heyd, J. J.; Brothers, E.; Kudin,

K. N.; Staroverov, V. N.; Kobayashi, R.; Normand, J.; Raghavachari, K.; Rendell, A.; Burant, J. C.; Iyengar, S. S.; Tomasi, J.; Cossi, M.; Rega, N.; Millam, J. M.; Klene, M.; Knox, J. E.; Cross, J. B.; Bakken, V.; Adamo, C.; Jaramillo, J.; Gomperts, R.; Stratmann, R. E.; Yazyev, O.; Austin, A. J.; Cammi, R.; Pomelli, C.; Ochterski, J. W.; Martin, R. L.; Morokuma, K.; Zakrzewski, V. G.; Voth, G. A.; Salvador, P.; Dannenberg, J. J.; Dapprich, S.; Daniels, A. D.; Farkas, O.; Foresman, J. B.; Ortiz, J. V.; Cioslowski, J.; Fox, D. J. *Gaussian 09*, revision A.1; Gaussian, Inc.: Wallingford, CT, 2009.

(46) Sun, W.; Zhu, H.; Barron, P. M. *Chem. Mater.* **2006**, *18*, 2602−2610.

(47) (a) Michalec, J. F.; Bejune, S. A.; Cuttell, D. G.; Summerton, G. C.; Gertenbach, J. A.; Field, J. S.; Haines, R. J.; McMillin, D. R. *Inorg. Chem.* **2001**, *40*, 2193−2200. (b) Shao, P.; Li, Y.; Sun, W. *J. Phys. Chem. A* **2008**, *112*, 1172−1179. (c) Chan, C.-W.; Cheng, L.-K.; Che, C.-M. *Coord. Chem. Rev.* **1994**, *132*, 87−97. (d) Cheung, T.-C.; Cheung, K.-K.; Peng, S.-M.; Che, C. M. *J. Chem. Soc., Dalton Trans.* **1996**, 1645−1651. (e) Cummings, S. D.; Eisenberg, R. *J. Am. Chem. Soc.* **1996**, *118*, 1949−1960. (f) Paw, W.; Lachiocotte, R. J.; Eisenberg, R. *Inorg. Chem.* **1998**, *37*, 4139−4141.

(48) (a) Siebert, R.; Winter, A.; Schubert, U. S.; Dietzek, B.; Popp, J. *Phys. Chem. Chem. Phys.* **2011**, *13*, 1606−1617. (b) Cheng, Y.-M.; Yeh, Y.-S.; Ho, M.-L.; Chou, P.-T.; Chen, P.-S.; Chi, Y. *Inorg. Chem.* **2005**, *44*, 4594−4603. (c) Siebert, R.; Winter, A.; Dietzek, B.; Schubert, U. S.; Popp, J. *Macromol. Rapid Commun.* **2010**, *31*, 883−888. (d) Qiu, D.; Guo, Y.; Wang, H.; Bao, X.; Feng, Y.; Huang, Q.; Zeng, J.; Qiu, G. *Inorg. Chem. Commun.* **2011**, *14*, 1520−1524. (e) Shao, P.; Li, Y.; Yi, J.; Pritchett, T. M.; Sun, W. *Inorg. Chem.* **2010**, *49*, 4507−4517. (f) Ji, Z.; Li, S.; Li, Y.; Sun, W. *Inorg. Chem.* **2010**, *49*, 1337−1346. (g) Xiang, H.; Zhou, L.; Feng, Y.; Cheng, J.; Wu, D.; Zhou, X. *Inorg. Chem.* **2012**, *51*, 5208−5212. (h) Simon, J. A.; Curry, S. L.; Schmehl, R. H.; Schatz, T. R.; Piotrowiak, P.; Jin, X.; Thummel, R. P. *J. Am. Chem. Soc.* **1997**, *119*, 11012−11022. (i) Dubinina, G. G.; Price, R. S.; Abboud, K. A.; Wicks, G.; Wnuk, P.; Stepanenko, Y.; Drobizhev, M.; Rebane, A.; Schanze, K. S. *J. Am. Chem. Soc.* **2012**, *134*, 19346−19349.

(49) Lees, A. J. *Comments Inorg. Chem.* **1995**, *17*, 319−346.

(50) (a) Sun, Y.; Joyce, L. E.; Dickson, N. M.; Turro, C. *Chem. Commun.* **2010**, *46*, 6759−6761. (b) Sun, Y.; Joyce, L. E.; Dickson, N. M.; Turro, C. *Chem. Commun.* **2010**, *46*, 2426−2428. (c) Liu, Y.; Hammitt, R.; Lutterman, D. A.; Joyce, L. E.; Thummel, R. P.; Turro, C. *Inorg. Chem.* **2009**, *48*, 375−385.

(51) (a) Liu, R.; Chen, H.; Chang, J.; Li, Y.; Zhu, H.; Sun, W. *Dalton Trans.* **2013**, *42*, 160−171. (b) Liu, R.; Dandu, N.; Li, Y.; Kilina, S.; Sun, W. *Dalton Trans.* **2013**, *42*, 4398−4409.

(52) Baba, A. I.; Ensley, H. E.; Schmehl, R. H. *Inorg. Chem.* **1995**, *34*, 1198−1207.